nature communications

Article

https://doi.org/10.1038/s41467-025-68047-y

A chromosome region linked to neurodevelopmental disorders influences locomotor behavior through sex-specific neural circuits

Received: 30 April 2024

Accepted: 16 December 2025

Published online: 03 January 2026

Check for updates

Jaekyoon Kim[1,2], Yann Vanrobaeys[1,2,3], Remya Rajan[4], M. Felicia Davatolhagh[5], Benjamin Kelvington[1,2], Snehajyoti Chatterjee[1,2], Sarah L. Ferri[2,6], Christopher Angelakos[7], Alea A. Mills[8], Marc V. Fuccillo[9], Kim T. Blackwell[4], Thomas Nickl-Jockschat[10,11,12] & Ted Abel[1,2,13]

Biological sex shapes the manifestation and progression of neurodevelopmental disorders (NDDs), however, the underlying mechanisms remains unclear. Hemideletion of the 16p11.2 region (16p11.2 del/+) is associated with NDDs, and 16p11.2 del/+ mice exhibit sex-specific, striatum-related phenotypes relevant to NDDs. In this study, using snRNA-seq, we identify cell type- and sex-specific transcriptomic changes in D1- and D2-spiny projection neurons (SPNs), with greater impact in males. Fiber photometry recordings reveal reduced neuronal activity in the dorsal striatum of 16p11.2 del/+ males, but not females, with D2-SPNs identified as the primary contributors to this reduction. Behaviorally, we utilize conditional genetic approaches and find that selective hemideletion in D2-SPNs, but not D1-SPNs, induces male-specific hyperactivity, whereas cortical hemideletion increases hyperactivity in both sexes. Thus, a locus linked to NDDs acts in distinct striatal circuits, selectively impacting behavior in a sex- and cell type-specific manner.

Male and female brains differ fundamentally in their reaction to genetic risk for brain disorders[1]. Sex differences in incidence, symptom presentation, and outcome have been found across biologically heterogeneous disorders, ranging from affective disorders to neurodegenerative diseases and primary brain tumors[2–4]. Neurodevelopmental disorders (NDDs), including autism spectrum disorders (ASD) and attention-deficit hyperactivity disorder (ADHD), provide a particularly striking example of sex-specific vulnerability, with male-to-female ratios of 4:1 ASD and 2:1 for ADHD[5,6]. Although the primary features of ASD are consistent across sexes, females can present differently than males, exhibiting fewer or harder-to-detect behavioral alterations[7,8]. This bias is most likely driven by a differential vulnerability of distinct

[1]Department of Neuroscience and Pharmacology, Carver College of Medicine, University of Iowa, Iowa City, IA, USA. [2]Iowa Neuroscience Institute, University of Iowa, Iowa City, IA, USA. [3]Interdisciplinary Graduate Program in Genetics, University of Iowa, Iowa City, IA, USA. [4]Roy J. Carver Department of Biomedical Engineering, University of Iowa, Iowa City, IA, USA. [5]Department of Neurobiology, David Geffen School of Medicine, University of California Los Angeles, Los Angeles, CA, USA. [6]Stead Family Department of Pediatrics, Carver College of Medicine, University of Iowa, Iowa City, IA, USA. [7]Department of Psychiatry and Behavioral Sciences, Stanford University School of Medicine, Stanford, CA, USA. [8]Cold Spring Harbor Laboratory, Cold Spring Harbor, Laurel Hollow, NY, USA. [9]Department of Neuroscience, University of Pennsylvania, Philadelphia, PA, USA. [10]Department of Psychiatry and Psychotherapy, Otto von Guericke University Magdeburg, Magdeburg, Germany. [11]German Center for Mental Health (DZPG), partner site Halle-Jena-Magdeburg, Berlin, Germany. [12]Center for Intervention and Research on adaptive and maladaptive brain Circuits underlying mental health (C-I-R-C), Halle-Jena-Magdeburg, Germany. [13]Department of Psychiatry, Carver College of Medicine, University of Iowa, Iowa City, IA, USA. e-mail: ted-abel@uiowa.edu

neuronal circuits to genetic risk factors[9,10], but identifying the exact underlying mechanisms remains a major challenge in the field.

Multiple lines of evidence have highlighted striatal circuits as key mediators of vulnerability to NDDs[11,12]. Neuroimaging studies in humans diagnosed with NDDs and in genetic mouse models have identified changes in striatal structure, function, and connectivity[12–14]. The striatum is a major hub that shapes an array of behaviors, including the regulation of locomotor activity[11,15]. Impairments in motor activity and stereotyped movements have been consistently observed in individuals diagnosed with NDDs[11,16]. The proper acquisition and execution of the locomotor behaviors demand a precisely honed interplay of striatal networks. In the striatum, two distinct neuronal circuits, the direct and indirect pathways, play a critical role in locomotion. The direct pathway is responsible for the initiation of actions and requires the activity of dopamine 1 receptor expressing spiny projection neurons (D1-SPNs), whereas the inhibitory indirect pathway recruits striatal dopamine 2 receptor expressing (D2-) SPNs[17,18]. Previous studies have suggested an imbalance between the direct and the indirect pathway in NDDs[11,19]; however, a comprehensive understanding of the role of these pathways in mediating sex-specific effects on behavior is lacking.

Here, we explore the mechanisms underlying the male preponderance of NDDs by mapping the sex-specific consequences of a copy number variation (CNV) linked to NDDs on the function of striatal circuits. We focus on 16p11.2 hemideletion (16p11.2 del/+), a rare genetic condition caused by a hemideletion within the chromosome 16p11.2 locus, as it is one of the most common genetic risk factors for NDDs[20,21]. Carriers of this CNV may receive a variety of diagnoses including ASD and ADHD[22,23]. Interestingly, female biological sex may be a protective factor for 16p11.2 del/+ carriers[24]. 16p11.2 del/+ model mice also show several sex-specific phenotypes[25,26], including behaviors dependent upon striatal circuits. Male mice demonstrate impairments in reward learning and motivation[27] and sleep[26], whereas hyperactivity is observed in both sexes[26]. Although previous studies have provided an initial indication of striatal circuit dysregulation in 16p11.2 del/+ mice[27,28], the exact underlying mechanisms of these phenotypes are not fully understood.

In this study, we examine the sex-specific impact of 16p11.2 del/+ on striatal circuits. High-throughput single-nucleus RNA sequencing (snRNA-seq) of neuronal nuclei from the striatum reveals that 16p11.2 del/+ induces distinct transcriptomic signatures in D1-SPNs and D2-SPNs between males and females. Furthermore, we observe sex- and cell type-specific changes in inhibitory synapse function of SPNs in 16p11.2 del/+ mice, supporting the selective impact of the mutation across distinct neuronal populations. GCaMP fiber photometry recordings reveal reduced dorsal striatal activity in 16p11.2 del/+ males, but not females, driven by D2-SPNs. Crucially, selective deletion of the 16p11.2 region in D2-SPNs induces hyperactivity in male but not in female mice indicating sexually dimorphic effects of the 16p11.2 region. Interestingly, 16p11.2 del/+ in the cortex is associated with hyperactivity in both sexes. Together, these results reveal that circuit level, sex-specific mechanisms mediate the behavioral alterations relevant to NDDs induced by 16p11.2 del/+.

Results

16p11.2 del/+ drives sex- and cell type-specific transcriptomic changes in SPNs

To delineate the impact of 16p11.2 del/+ on specific neuronal circuits in the striatum, we first examine the transcriptomic landscape at the single cell level using snRNA-seq (Fig. 1A). In a previous study, single-cell gene expression was analyzed using multiplex single cell-qPCR[28]. However, neonatal brains from 16p11.2 del/+ mice were studied, and sex information was not provided. Here, we investigate cell type-specific transcriptomic changes in the striatum of both male and female 16p11.2 del/+ and wild-type (wt) adult mice. Based on the transcriptional signature, we identify sub-populations of striatal neurons, including direct pathway spiny projection neurons (D1-SPNs), and indirect pathway spiny projection neurons (D2-SPNs), as well as various cortical neurons (Fig. 1B, S1, S2, S3). D1- and D2-SPNs exhibit marked transcriptional differences between 16p11.2 del/+ and wt mice that differ between the sexes. In D1-SPNs, we find 99 differentially expressed genes (DEGs) between 16p11.2 del/+ and wt males compared to 18 in females, whereas in D2-SPNs, we identify 114 DEGs in males compared to 20 in females (Fig. 1C–H, and supplementary data 1–4). These results suggest a differential impact of hemideletion of genes in 16p11.2 region on male and female SPNs, with a ~ 5-fold greater impact in males. In males, 58 DEGs are shared by both types of striatal neurons (Fig. 1I). Importantly, genes whose expression is altered by the 16p11.2 del/+ are enriched in genes associated with ASD. Using the SFARI gene database, we find that 21 DEGs in D1-SPNs of 16p11.2 del/+ male mice overlapped with ASD risk genes, and 21 DEGs in D2-SPNs overlapped with ASD risk genes, including 12 overlapping genes in both types of SPNs (Fig. 1I, S3). Among these 30 genes, several, such as *Adcy5*, *Camk2b*, *Herc1*, *Grin2b*, *Ube3a*, *Lrp1*, and *Elavl3*, have been reported to be associated with motor function[29–35].

16p11.2 del/+ leads to distinct changes in synaptic properties in D1-SPNs and D2-SPNs

To characterize the molecular functions of the DEGs from D1- and D2-SPNs on male 16p11.2 mice, we perform pathway analysis. GO enrichment network analysis reveals that genes differentially expressed in both D1- and D2-SPNs (58 DEGs) are associated with regulation of excitatory postsynaptic organization (Fig. 2A). This is consistent with previous reports of increased miniature excitatory postsynaptic currents (mEPSC) frequency and increased AMPAR/NMDAR ratio in 16p11.2 del/+ SPNs[28], suggesting both pre- and postsynaptic alterations at excitatory synapses. Interestingly, there is a substantial enrichment of genes associated with gamma-aminobutyric acid (GABA) synaptic transmission among the 41 exclusive D1-SPNs DEGs (Fig. 2A). To determine whether these molecular changes are reflected at the synaptic level, we investigate inhibitory synaptic function by recording inhibitory postsynaptic currents (IPSC). This reveals region- and sex-specific effects. In the dorsal striatum, we observe decreased spontaneous IPSC (sIPSC) frequency in D2-SPNs of 16p11.2 del/+ males (Fig. 2B–E) and increased sIPSC amplitude in D1-SPNs of 16p11.2 del/+ females (Fig. 2F–I). Additionally, miniature IPSC (mIPSC) recordings in the nucleus accumbens (NAc) reveal distinct alterations in D1- and D2-SPNs of 16p11.2 del/+ male mice. Comparison of mIPSC amplitudes shows a significant reduction in D1-SPNs of NAc in male 16p11.2 del/+ mice versus wt mice, indicating decreased postsynaptic GABAergic responsiveness (figure S4A-B). However, mIPSC frequency is significantly reduced in D2-SPNs of NAc in 16p11.2 del/+ males (figure S4C-D), similar to observations in D2-SPNs of the dorsal striatum. This suggests decreased presynaptic GABA release or fewer inhibitory inputs onto D2-SPNs across striatal subregions. Together, these results highlight the differential impact of the high-risk polygenic factor 16p11.2 del/+ on molecular pathways and inhibitory synaptic transmission within the two major neuronal circuits in the striatum, with region- and sex-specific alterations pointing to circuit-specific vulnerability.

Sex-specific transcriptomic changes in 16p11.2 del/+ male mice correlate with wildtype gene expression differences between sexes

To explore the effects of baseline sex differences on gene expression changes in male 16p11.2 del/+ mice, we compare gene expression between wt males and wt females to gene expression between wt males and 16p11.2 del/+ males (figure S5A, B). As expected, there are substantial baseline transcriptional differences between wt males and females. Interestingly, differentially expressed genes in 16p11.2 del/+

https://doi.org/10.1038/s41467-025-68047-y

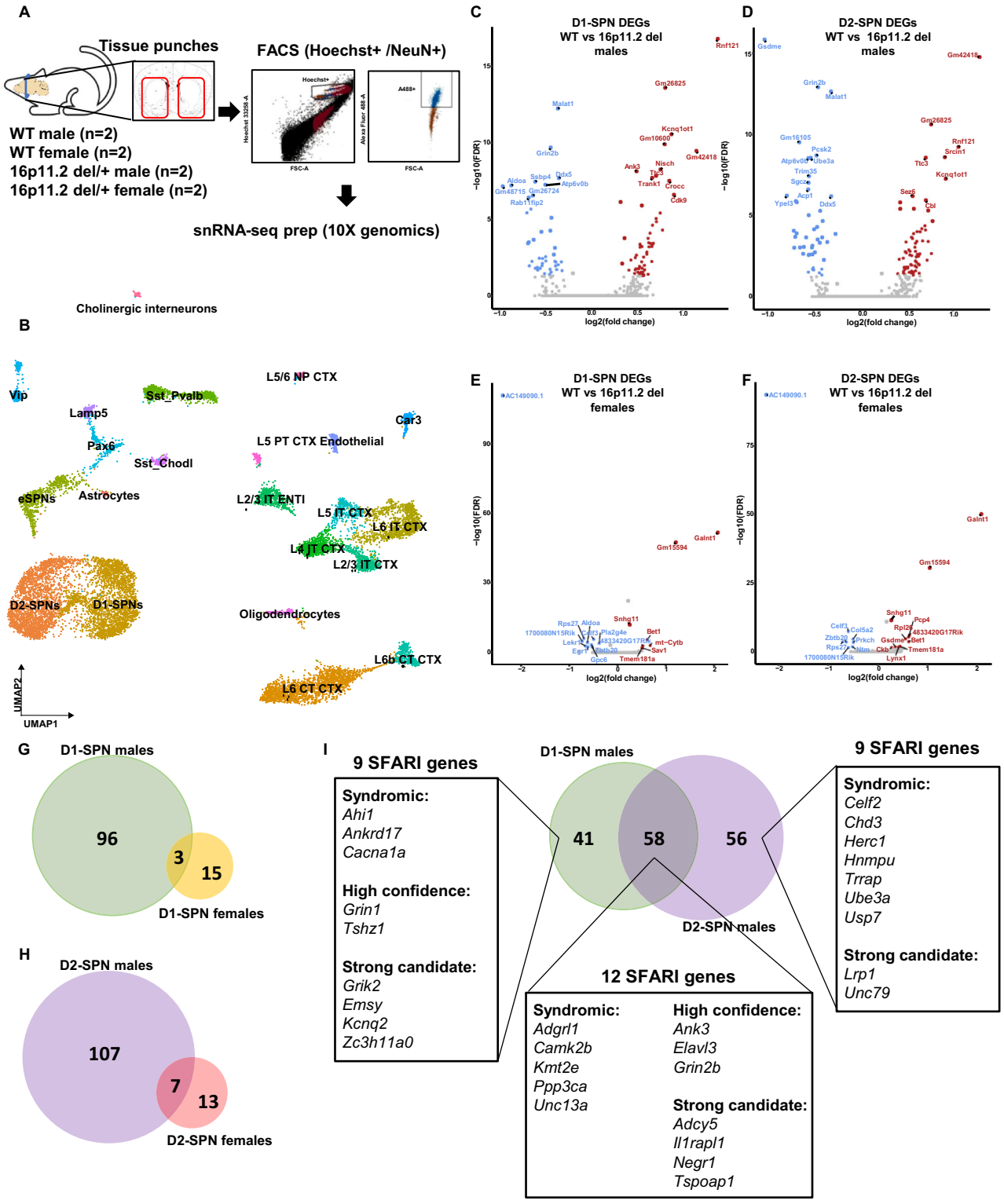

male mice show a positive correlation with genes more highly expressed in wt females, suggesting that the deletion in males induces a partial shift toward a more female-like transcriptional profile. We perform the same analysis in 16p11.2 del/+ females using a quadrant plot approach (figure S5C, D). However, due to the smaller number of DEGs in females, the results were less conclusive. To investigate whether these gene expression patterns are specific to SPNs or observed more generally in the striatum, we analyze mRNA-seq data from a previous study (GSE224750) from the striatum of both male and female young adult 16p11.2 del/+ and wt mice (figure S5E, F). Consistent with our SPN-specific results, the transcriptomic changes in 16p11.2 del/+ males again positively correlate with baseline female-biased expression (figure S5E). In contrast, female gene expression changes induced by 16p11.2 del/+ appear less influenced by baseline sex differences (figure S5F). To ensure that each animal is treated as an independent replicate, we perform pseudobulk differential expression analysis by aggregating counts within each cell type and sample. This approach confirms the correlations between sex effects and 16p11.2

Fig. 1 | 16p11.2 del/+ drives sex- and cell type- specific transcriptomic changes in the striatum. A snRNA-seq preparation procedure. Tissue was harvested from male and female wt and 16p11.2 del/+ mice ($n = 2$). Dissection boundaries are indicated by red lines on the schematic illustrations[70]. **B** Cell type annotation of the different cluster of neurons from the striatum and adjacent regions projected on a two-dimensional uniform approximation and projection (UMAP) map. The different clusters of cell types are labeled by their cell type identification name. **C**, **D** Differentially expressed genes in D-1 SPNs (**C**) and D2-SPNs (D) in 16p11.2 del/+ male mice compared to wt mice are displayed in volcano plots of statistical significance (in -log10) against fold-change (in log2) of gene expression change. Genes with a false discovery rate (FDR) < 0.05 are highlighted in red (upregulated) and blue (downregulated) for significantly regulated genes. **E**, **F** Differentially expressed genes in D1-SPNs (**E**) and D2-SPNs (**F**) in 16p11.2 del/+ female mice compared to wt mice are displayed in volcano plots. **G**, **H** Venn diagram representing the number of overlapping DEGs (adjusted p-value < 0.05 and log2FC > |0.25 |) in D1-SPNs (**C**, **E**) or in D2-SPNs (**D**, **F**) of 16p11.2 del/+ mice relative to wt mice. The observed overlaps are significantly greater than expected by chance, based on the exact hypergeometric probability test ($p < 1.325e-04$ for **G**; $p < 2.871e-11$ for I). (I) Venn diagram representing the overlap of significant DEGs (male D1- and D2-SPNs) from this study with the SFARI Gene autism susceptibility database focusing on the human gene module. The overlap is highly significant ($p < 2.355e-107$). The overlapping genes are represented in the pie charts according to their respective score developed by SFARI.

genotype effects (figure S5G, H), consistent with our single-cell results. Together, these findings highlight robust baseline transcriptional differences between wt males and females and suggest that 16p11.2 del/+ males may engage a compensatory transcriptional response, further supporting the idea that females possess a more resilient molecular baseline to the effects of the deletion.

Neuronal activity frequency in D2-SPNs is reduced in male 16p11.2 del/+ mice

To measure in vivo neuronal population activity within striatal circuits, we deliver AAV-syn-jGCaMP7f-WPRE to the dorsal striatum, a region associated with locomotor regulation. Two weeks after surgery, mice exhibit robust jGCaMP7f expression in the dorsal striatum (Fig. 3A). During open-field exploration, we record jGCaMP7f signals to monitor neuronal activity (Fig. 3B, C). Spike detection analysis reveals the frequency of striatal neuronal activity events (Fig. 3D). We observe a significant reduction in neuronal activity in male 16p11.2 del/+ mice compared to wt males (Fig. 3E), but not in female 16p11.2 del/+ mice (Fig. 3F). The AAV-ENK-CRE virus expresses CRE recombinase under the control of the enkephalin promoter, which is specific to D2-SPNs, while the AAV9-PPTA-CRE virus uses the preprotachykinin A promoter to drive CRE expression specifically in D1-SPNs[36,37]. By co-injecting AAV-ENK-CRE with either AAV-FLEX-tdTomato or AAV-FLEX-GFP, or AAV-PPTA-CRE with either AAV-FLEX-tdTomato or AAV-FLEX-GFP into D2-GFP or D1-tdTomato reporter mice, we confirm that AAV-ENK-CRE and AAV-PPTA-CRE drive expression exclusively in D2-SPNs and D1-SPNs, respectively (Fig. 3G–N). By applying AAV-ENK-CRE and AAV-PPTA-CRE in combination with AAV-syn-FLEX-jGCaMP8m-WPRE in 16p11.2 del/+ mice, we can monitor D2-SPN and D1-SPN activity simultaneously in each hemisphere of the brain (Fig. 3O). Two weeks after surgery, mice show robust jGCaMP8m expression with each CRE-expressing virus in the dorsal striatum (Fig. 3P, Q). We observe a significant reduction in D2-SPN activity in male 16p11.2 del/+ mice compared to wt males, while D1-SPN activity remains unchanged (Fig. 3R). These results demonstrate a sex-specific and circuit-specific impact of the 16p11.2 deletion on striatal neuronal activity.

16p11.2 del/+ in D2-SPNs leads to hyperactive behavior in male mice

To determine the impact of 16p11.2 del/+ on behavior linked to distinct striatal circuits, we utilize conditional genetic approaches to introduce the hemideletion selectively in either D1- or D2-SPNs. We generate mice with 16p11.2 del/+ exclusively in D2-SPNs by crossing 16p11.2 flox/+ mice and A2A-CRE + /- mice (Fig. 4A). Double positive mice (flox/+**:**CRE + /-; A2A-CRE x 16p11.2 flox, D2-16p11.2 del/+ mice) are considered as the experimental group and the other three groups of mice (+/+**:**CRE-/-, flox/+**:**CRE-/-, + / + **:**CRE + /-) are combined as controls. Young adult (3–4-month-old) male and female D2-16p11.2 del/+ mice and littermate control mice are monitored in the home-cage using an infrared beam-break system across the 24-hour cycle, similar to previous studies[26]. We find increased activity in male (Fig. 4B, C, S6A) but not female (Fig. 4D, E, S6B) D2-16p11.2 del/+ mice, in contrast to our findings of hyperactivity in both sexes in the whole-organism 16p11.2 del/+ (figure S7)[26]. These results demonstrate that 16p11.2 del/+ in D2-SPNs induces hyperactive behavior specifically in male mice, revealing circuit level sex differences of the deletion of 16p11.2 region, consistent with our gene expression data.

To characterize the impact of 16p11.2 del/+ selectively in D1-SPNs, we generate mice with the hemideletion specifically in D1-SPNs by crossing 16p11.2 flox/+ mice and D1-CRE + /- mice (Fig. 4F). Again, double positive mice (flox/+**:**CRE + /-; sD1-CRE x 16p11.2 flox, D1-16p11.2 del/+ mice) are considered as the experimental group and the other three littermate genotypes (+/+**:**CRE-/-, flox/+**:**CRE-/-, + / + **:**CRE + /-) are categorized as the control group for behavioral tasks. Both male (Fig. 4G, H, S6C) and female (Fig. 4I, J, S6D) D1-16p11.2 del/+ mice exhibit similar locomotor activity to littermate controls. We confirm that neither 16p11.2 flox mice, D1-CRE mice, nor A2A-CRE mice exhibit hyperactive locomotion (figure S6, S8). Together, our results reveal that the sexually dimorphic effects of 16p11.2 del/+ on D2-SPNs mediates NDD-relevant increases in the locomotor activity of male animals.

Moreover, we find that sulpiride, a selective D2 receptor antagonist, alleviates hyperactivity in 16p11.2 del/+ male mice to levels comparable to those of wt males (Fig. 5A, B, S9). Although sulpiride also reduces locomotor activity or shows a trend toward reduction in wt males, wt females, and 16p11.2 del/+ females (Fig. 5C-H), effect size analysis reveals the strongest impact in 16p11.2 del/+ males (Cohen's $d = 1.10$), compared to smaller effects in wt males ($d = 0.58$), wt females ($d = 0.64$), and 16p11.2 del/+ females ($d = 0.64$). Interestingly, risperidone, a potent antagonist of D2 and 5-HT receptors, alleviates hyperactivity in both male and female 16p11.2 del/+ mice (figure S10A–D), with a larger effect size observed in females. Effect size analysis shows the strongest impact in 16p11.2 del/+ females (Cohen's $d = 0.80$), compared to 16p11.2 del/+ males ($d = 0.60$), wt males ($d = 0.26$), and wt females ($d = 0.04$), suggesting sexual dimorphism in the regulation of locomotor activity. In contrast, treatment with SCH39166, a D1 receptor antagonist, does not alleviate hyperactivity in either 16p11.2 del/+ males or wt males (figure S11), further supporting a key role for D2-SPNs in driving hyperactive behavior in 16p11.2 del/+ males. Together, these findings highlight D2-SPNs as a critical circuit component underlying hyperactivity in males, but not females, suggesting sex-specific mechanisms driving this behavioral phenotype.

16p11.2 del/+ in D2-SPNs in the dorsal lateral striatum drives hyperactive behavior in male mice

Distinct behavioral roles have been characterized for specific subregions within the striatum, with the dorsal medial striatum (DMS) supporting more cognitive functions and the dorsal lateral striatum (DLS) supporting motor output[11,38]. However, the conditional genetic approaches using D1-CRE and A2A-CRE mice lack the specificity necessary to target neuronal circuits within specific subregions of the striatum. To target specific subregions within the striatum, we deliver AAV-ENK-CRE virus to striatal subregions in 16p11.2 flox/+ male mice. Injecting this virus in 16p11.2 flox mice localizes the 16p11.2

https://doi.org/10.1038/s41467-025-68047-y

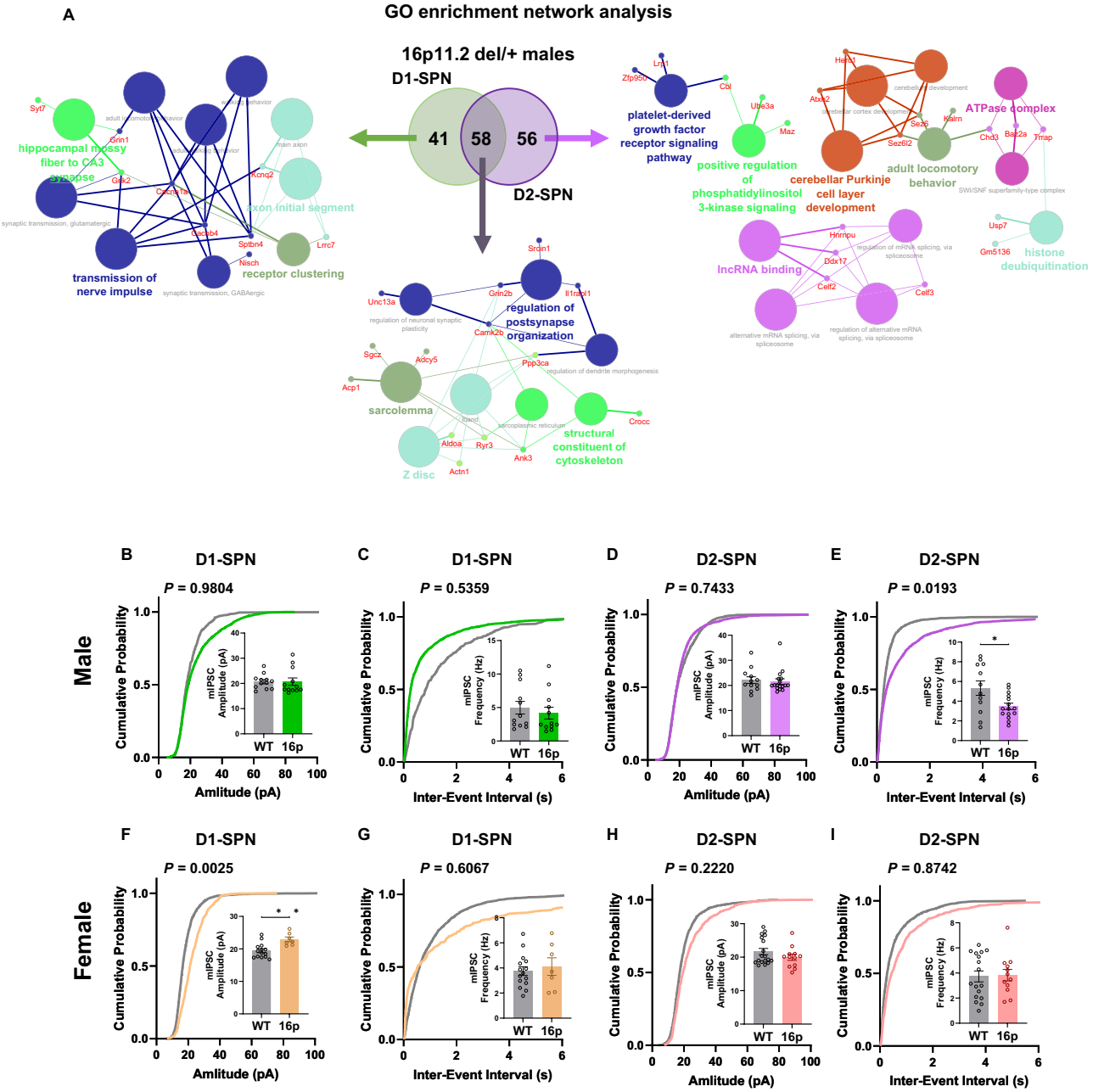

Fig. 2 | 16p11.2 del/+ induces distinct changes in synaptic function in D1-SPNs and D2-SPNs in male mice. A Venn diagram representing the overlap of significant DEGs without the genes inside or near the 16p11.2 region between the D1-SPNs and D2-SPNs. Pathway analysis using ClueGo (KEGG and GO: Molecular function terms) of the male DEGs from either only D1-SPNs, only D2-SPNs or both D1-SPNs and D2-SPNs. Only pathways with a corrected *p* value (Bonferroni step down) under 0.05 are displayed. The genes are labeled using CluePedia and are represented next to circles filled with either blue or red color to show the directionality of the dysregulation (blue=down-regulated; red=up-regulated). **B**, **C** Recording of synaptic events in dorsal striatum D1-SPNs of male 16p11.2 del/+ mice ($n = 12$ wt cells from 5 animals, $n = 12$ 16p11.2 del/+ cells from 6 animals) show sIPSC amplitude and frequency remained unchanged ($p = 0.9804$, **B**; $p = 0.5359$, (**C**). **D**, **E** Recording of synaptic events in dorsal striatum D2-SPNs of male 16p11.2 del/+ mice ($n = 12$ wt cells from 5 animals, $n = 15$ 16p11.2 del/+ cells from 6 animals) show reduced sIPSC frequency ($p = 0.0193$, (**E**) with comparable sIPSC amplitude ($p = 0.7433$, (**D**). **F**, **G** Recording of synaptic events in dorsal striatum D1-SPNs of female 16p11.2 del/+ mice ($n = 15$ wt cells from 7 animals, $n = 8$ 16p11.2 del/+ cells from 5 animals) show increased sIPSC amplitude ($p = 0.0025$, (**F**), while sIPSC frequency remained unchanged ($p = 0.6067$, (**G**). **H**, **I** Recording of synaptic events in dorsal striatum D2-SPNs of female 16p11.2 del/+ mice ($n = 18$ wt cells from 7 animals, $n = 12$ 16p11.2 del/+ cells from 4 animals) show sIPSC amplitude and frequency remained unchanged ($p = 0.2220$, H; $p = 0.8742$, (**I**). Error bars represent SEM. Statistical comparisons are performed using unpaired two-tailed t-tests. $^{*}p < 0.05$, $^{**}p < 0.01$. Source data are provided as a Source Data file for panels (**B**–**I**).

hemideletion effects to D2-SPNs within specific striatal subregions. We co-inject a mix of AAV-ENK-CRE and AAV-flex-tdTomato in wt and 16p11.2 flox/+ male mice in three different striatal regions: the DMS, DLS, and NAc, and examine the impact on locomotor activity (Fig. 6A). Activity monitoring data shows that hyperactivity resulted from 16p11.2 del/+ in D2-SPNs in the DLS (Fig. 6C, D), but not in the DMS or NAc (Fig. 6F, G, I, J). Following behavioral testing, brains are collected, and we confirm hemideletion of the 16p11.2 region in the striatum using PCR and verify injection location and the extent of viral expression using fluorescent microscopy (Fig. 6B, E, H, S13). In sum,

https://doi.org/10.1038/s41467-025-68047-y

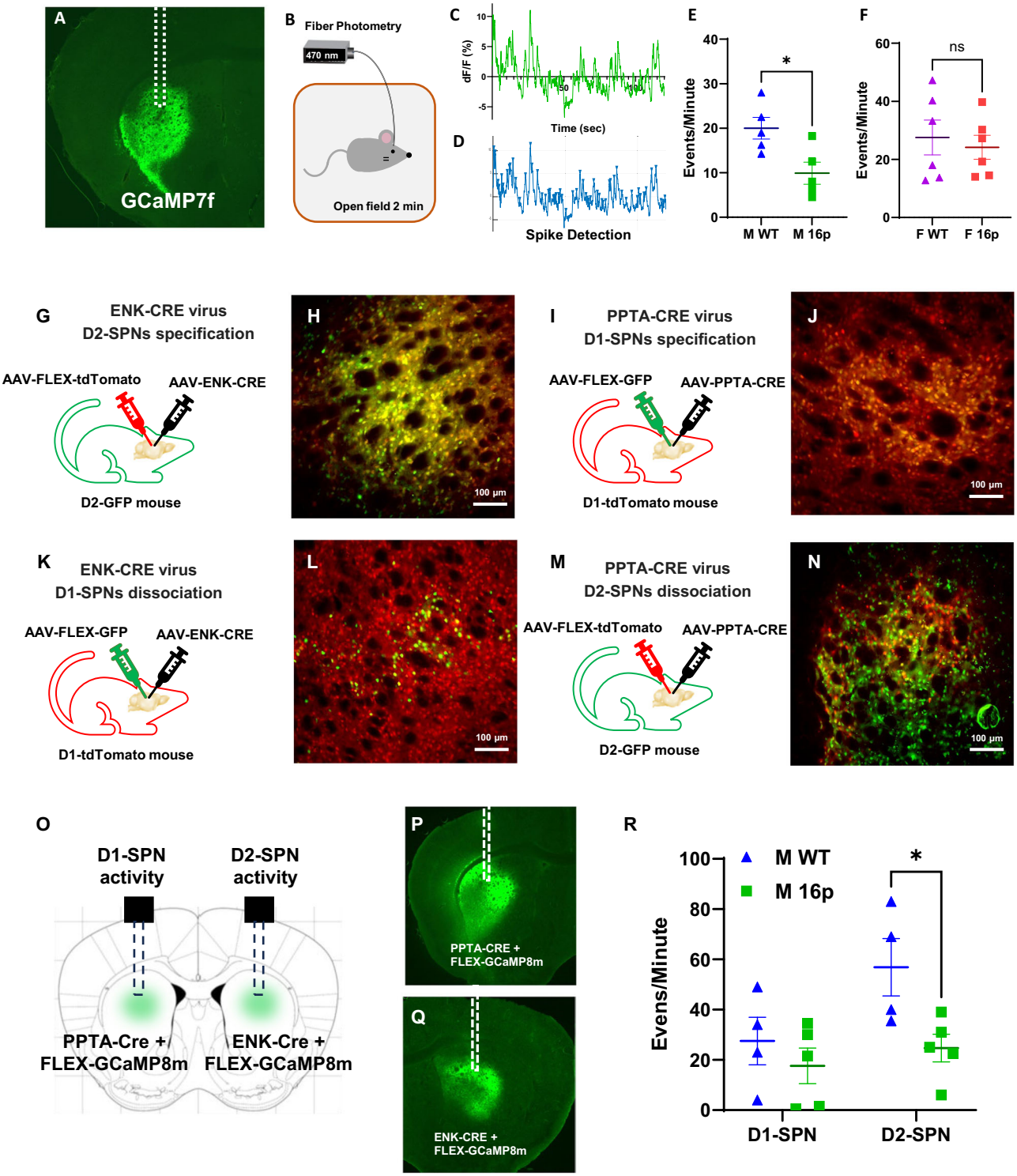

these results demonstrate that 16p11.2 del/+ in D2-SPNs, specifically of the DLS, induces hyperactive behavior in male mice.

16p11.2 del/+ in the cortex causes hyperactivity in both male and female mice

16p11.2 del/+ in D2-SPNs drives hyperactive behavior only in male mice, suggesting sexual dimorphism on the circuit level. However, the circuit basis for the hyperactivity observed in whole-organism 16p11.2 del/+ female mice (figure S7B[26]), remains unresolved. We hypothesize that a loss of the 16p11.2 region in neurons within the cortex, one of the main excitatory inputs into the striatum, contributes to hyperactivity in female 16p11.2 del/+ mice. To explore the functional role of genes in the 16p11.2 region in the cortex, we cross EMX1-CRE mice and 16p11.2 flox/+ mice (Fig. 7A). As before, double positive mice (flox/+:CRE + /-; EMX1-CRE x 16p11.2 flox, Ctx-16p11.2 del/+ mice) are considered as the experimental group and the other three genotypes (+/+:CRE-/-, flox/+:CRE-/-, + / + :CRE + /-) are combined as controls. Remarkably, both male (Fig. 7B, C) and female (Fig. 7D, E) Ctx-16p11.2 del/+ mice display hyperactive behavior compared to sex-matched control mice, phenocopying the 16p11.2 del/+ mice hyperactivity observed in both sexes (figure S7)[26]. These behavioral results demonstrate that deletion of the 16p11.2 region differentially impacts various hubs within cortico-

Fig. 3 | Male 16p11.2 del/+ mice display a reduced frequency of neuronal activity in D2-SPNs. A Representative fluorescence microscope images of AAV-syn-jGCaMP7f-WPRE expression under 2.5x. **B** Fiber photometry recording during open field for 2 min. **C** Representative GCaMP signaling after %ΔF/F calculation. The isosbestic signal is fit with a biexponential decay and used to normalize the fluorescence trace. **D** Representative spike detection analysis (minimum peak prominence of 1). **E**, **F** Recording of GCaMP7f events in dorsal striatum ($n = 5$ wt, $n = 5$ 16p11.2 del/+) show decreased event frequency ($p = 0.0196$, **E** in male 16p11.2 del/+ mice, while female 16p11.2 del/+ mice remained unchanged ($p = 0.6532$, **F**). Statistical comparisons are performed using unpaired two-tailed t-tests. **G** Schematic illustrating the virus mix injection of AAV-ENK-CRE and AAV-FLEX-tdTomato into the striatum of D2-GFP mouse. **H** Representative fluorescence microscope images of AAV-ENK-CRE and AAV-FLEX-tdTomato expression on D2-GFP mouse striatum (under 20x). ENK virus expression (red) is colocalized to D2-SPNs (green, ~90% colocalization). Scale bar indicates 100 μm. **I** Schematic illustrates the virus mix injection of AAV-PPTA-CRE and AAV-FLEX-GFP into the striatum of D1-tdTomato mouse. **J** Representative fluorescence microscope images of AAV-PPTA-CRE and AAV-FLEX-GFP expression on D1-tdTomato mouse striatum (under 20x). PPTA virus expression (green) is colocalized to D1-SPNs (red, ~90% colocalization). **K** Schematic illustrates the virus mix injection of AAV-ENK-CRE and AAV-FLEX-GFP into the striatum of D1-tdTomato mouse. **L** Representative fluorescence microscope images of AAV-ENK-CRE and AAV-FLEX-GFP expression on D1-tdTomato mouse striatum (under 20x). ENK virus expression (green) is dissociated to D1-SPNs (red, less than 15% colocalization). **M** Schematic illustrates the virus mix injection of AAV-PPTA-CRE and AAV-FLEX-tdTomato into the striatum of D2-GFP mouse. **N** Representative fluorescence microscope images of AAV-PPTA-CRE and AAV-FLEX-tdTomato expression on D2-GFP mouse striatum (under 20x). PPTA virus expression (red) is dissociated to D2-SPNs (green, less than 15% colocalization). **O** Schematic illustrations show GCaMP signals recorded from the dorsal striatum of male mice using cell type-specific expression driven by AAV-PPTA-CRE or AAV-ENK-CRE, along with FLEX-GCaMP8m delivered to each hemisphere for simultaneous recordings, based on the mouse brain coronal section atlas[70]. **P**, **Q** Representative fluorescence microscope images of AAV-PPTA-CRE (**P**) or AAV-ENK-CRE (**Q**), along with FLEX-GCaMP8m expression (under 2.5x). **R** Recordings of GCaMP8m events in D1-SPNs ($n = 4$ WT, $n = 5$ 16p11.2 del/+) show a main effect of genotype, $F(1, 14) = 6.475$, $p = 0.0234$; a main effect of cell type, $F(1, 14) = 4.866$, $p = 0.0446$; and no significant genotype x cell type interaction, $F(1, 14) = 1.815$, $p = 0.1993$, in two-way ANOVA. Fisher's LSD post-hoc tests indicate D2-SPNs exhibit a significantly decreased frequency of neuronal activity in 16p11.2 del/+ males ($p = 0.0156$). Error bars represent SEM. $^*p < 0.05$. Source data are provided as a Source Data file for (**E**, **F**, **R**).

striatal circuits, suggesting that circuit level sex differences mediate behavioral phenotypes of NDDs.

Discussion

In this study, we describe sex-specific contributions of the 16p11.2 del/+ region to the molecular, cellular, and behavioral aspects of striatal circuits. Single-cell level transcriptomic analysis reveals substantial sex differences in the impact of 16p11.2 del/+ on D1- and D2-SPNs, as well as differences across other cell types. D2-SPN calcium event frequency is reduced in male 16p11.2 del/+ mice. Conditional 16p11.2 del/+ in specific striatal circuits and in specific striatal subregions induces hyperactivity in a sex-specific manner, indicating sexually dimorphic effects of the genes in the 16p11.2 region on the function of distinct neuronal circuits within the striatum, underlying hyperactivity in 16p11.2 del/+ mice.

Conditional 16p11.2 del/+ in distinct striatal pathways reveals circuit-level sex differences. Given the hyperactive behavior of 16p11.2 del/+ mice in both sexes, it is noteworthy that 16p11.2 del/+ in D2-SPNs drives different locomotor behavior phenotypes between male and female mice. These results indicate that 16p11.2 del/+ in D2-SPNs is a critical driver of hyperactive behavior in males, but not in females, revealing circuit-level sex differences underlying hyperactivity in 16p11.2 del/+ mice. This is significant because it implies that even when male and female mice exhibit the same behavioral phenotype, different neuronal circuits may underlie this phenotype in males and females. There has been substantial interest in profiling sex differences in striatal anatomy and function. Clinical reports have shown sex differences in dopamine release at baseline in the ventral striatum[39]. In rodent models, it has been reported that dopamine release and uptake dynamics, as well as the expression of dopamine receptors in the striatum, differ depending on sex[40,41]. Additionally, several preclinical studies have shown sex-dependent responses to psychostimulants in the striatum[40,42]. Sex differences in the distribution and density of striatal interneurons are also reported[43]. Our findings reveal that the 16p11.2 del/+ exerts sexually dimorphic effects at the circuit level and elicits differential responses to pharmacological treatments. The distinct effects of sulpiride and risperidone further support this notion, with sulpiride showing greater efficacy in males and risperidone having a stronger impact in females. Given that sulpiride, a selective D2 receptor antagonist, produced a larger effect in 16p11.2 del/+ males, we speculate that 5-HT receptor antagonism may play a more prominent role in mediating behavioral effects in 16p11.2 del/+ females. This interpretation is supported by prior findings that hyperactivity in females requires cortical deletion, consistent with the high expression of 5-HT receptors in the mouse cortex[44]. Together, these results highlight the importance of developing sex-specific therapeutic strategies, even for individuals who display similar behavioral outcomes stemming from the same genetic mutation. Further support for sex-specific circuit effects that define behavior is provided by our finding that 16p11.2 del/+ in cortical excitatory neurons phenocopy whole-organism 16p11.2 del/+ mice hyperactivity observed in both sexes. These findings indicate that deletion of the 16p11.2 region has a differential impact on key hubs within cortico-striatal circuits in a sex-specific manner. The striatum receives a complex array of sensory and contextual information from cortical afferents, and the behavioral outputs are subject to the input sent from cortical regions that the striatum receives[38,45]. Moreover, a recent study showed that disruption of the hyper-direct pathway, a circuit of cortico-subthalamic projections bypassing the striatum, induces hyperactive behavior in mice[46]. Therefore, investigating the cortex-specific mechanisms underlying male and female hyperactivity will provide further insight into the circuit-level sex differences mediating hyperactive behavior in 16p11.2 del/+ mice.

D2-SPNs are a critical driver of hyperactive behavior in 16p11.2 del/+ males. The traditional rate model of movement control suggests that the two major neuronal circuits in the striatum antagonize each other: the direct pathway (D1-SPNs) initiates movement, while the indirect pathway (D2-SPNs) suppresses it[17,18]. However, recent studies have challenged this view, providing evidence that both pathways are activated during the initiation of movements, suggesting that the coordinated activity of both pathways is necessary for the control of movement[47,48]. Our results show that 16p11.2 del/+ in D2-SPNs, but not in D1-SPNs, induces hyperactive behavior in male mice. Additionally, we discover reduced neuronal activity in the dorsal striatum of 16p11.2 del/+ male mice, but not in 16p11.2 del/+ female mice, is driven by D2-SPNs. The observation that systemic administration of a D2 receptor antagonist, sulpiride, reduces hyperactivity in 16p11.2 del/+ male mice further supports the idea that excessive or dysregulated D2 receptor signaling contributes to the behavioral phenotype, likely by exacerbating the suppression of D2-SPN activity. Together, these findings underscore the pivotal role of D2-SPNs in the dorsal striatum as a key contributor to hyperactivity in 16p11.2 del/+ males.

Altered D2-SPN activity in the dorsal striatum may contribute to NDD-relevant behaviors beyond general locomotion. The dorsal striatum and its D2-SPNs are strongly implicated in habit formation and the expression of stereotyped behaviors, domains that may be

https://doi.org/10.1038/s41467-025-68047-y

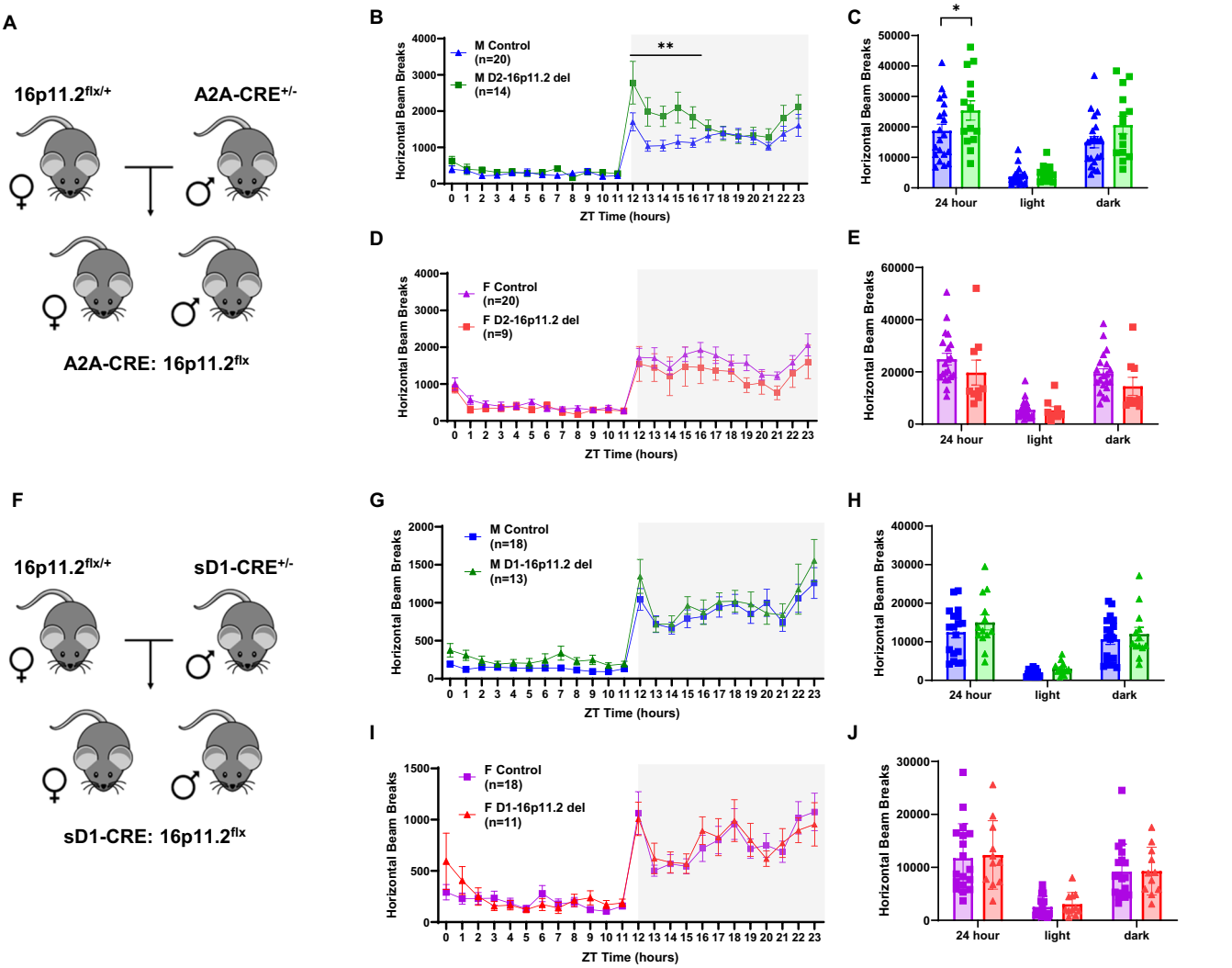

Fig. 4 | D2-SPN-specific 16p11.2 del/+ mediates hyperactive behavior in males. **A** Genetic crosses used to induce 16p11.2 del/+ to D2-SPNs. **B**–**E** Activity monitoring shows increased activity in male A2A-CRE x 16p11.2 flox mice. **B** Main effect of genotype, F(1, 32) = 3.218, $p = 0.823$; main effect of time, F(23, 736) = 36.33, $p < 0.001$; genotype x time interaction, F(23, 736) = 2.694, $p < 0.001$; RM two-way ANOVA with no correction. Post hoc shows significant differences between male A2A-CRE x 16p11.2 flox mice and control littermates in 12-16 h time slots. **C** 24-h plot shows increased activity in male A2A-CRE x 16p11.2 flox mice (t = 2.287, $p = 0.0244$; n = 20 control, $n = 14$ D2-16p11.2 del). **D** Main effect of genotype, F(1, 27) = 1.263, p = 0.2710; main effect of time, F(23, 621) = 22.20, $p < 0.001$; genotype x time interaction, F(23, 621) = 0.5083, p = 0.9738. **E** No change is reported in post hoc ($n = 20$ control, $n = 9$ D2-16p11.2 del). **F** Genetic crosses used to induce 16p11.2 del/+ from D1-SPNs. **G**–**J** Activity monitoring results show equal locomotor activity regardless of genotypes in males (**G**, **H**) and females (**I**, **J**). Gray box indicates the dark cycle and mice activities are presented in 1-h bins (**G**, **I**). Mice activities are plotted by light/dark cycle (**H**, **J**). **G** Main effect of genotype, F (1, 29) = 1.137, $p = 0.2950$; main effect of time, F(23, 667) = 37.81, $p < 0.001$; genotype x time interaction, F(23, 667) = 0.4637, $p = 0.9856$. **H** No change is detected in post hoc ($n = 18$ control, $n = 13$ D1-16p11.2 del). **I** Main effect of genotype, F(1, 27) = 0.06053, $p = 0.8075$; main effect of time, F(23, 621) = 25.27, $p < 0.001$; genotype x time interaction, F(23, 621) = 0.6693, $p = 0.8773$. **J** No change is detected in post hoc ($n = 18$ control, $n = 11$ D1-16p11.2 del). Error bars represent SEM. $^*p < 0.05$, $^{**}p < 0.01$. Source data are provided as a Source Data file for (**B**–**E**, **G**–**J**).

more directly relevant to the restricted and repetitive behaviors observed in NDDs. Prior studies have shown that decreased D2-SPN activity in the DLS facilitates habit consolidation and suppresses previously learned goal-directed responses[49]. Given our finding of reduced D2-SPN activity in the dorsal striatum of male 16p11.2 del/+ mice, future experiments should investigate whether this circuit dysfunction contributes to behavioral rigidity or stereotypy.

Conditional 16p11.2 del/+ in the DLS, but not the DMS, induces hyperactivity in males. Distinct roles have been proposed for the DLS and the DMS: the DLS is linked to habitual actions, while the DMS is associated with goal-directed behavior[38]. These distinct roles are associated with unique striatal afferent connections: Somatic sensorimotor subnetworks extend their projections into the DLS, while associative cortical areas, such as anterior cingulate cortex and prelimbic cortex, project into the DMS[11,38,45]. In line with the distinct roles of the DLS and the DMS, our study reveals that 16p11.2 del/+ within D2-SPNs of the DLS, but not the DMS, results in hyperactive behavior. While we demonstrate the impact of genetic variations linked to NDDs on these subregions regarding behavioral phenotypes, the molecular impact of these genetic variations on striatal subregions, specifically the DMS and DLS, remain unexamined. To address this gap, future experiments, such as spatial transcriptomics, are essential for a comprehensive characterization of region-specific phenotypes.

snRNA-seq analysis emphasizes the significance of polygenic influences of ASD risk genes. Recent research underscores the notion that transcriptomic patterns of brain disease risk genes offer a unique molecular signature specific to each disorder[50]. Additionally, there are indications that multiple genes within the 16p11.2 region may exert

https://doi.org/10.1038/s41467-025-68047-y

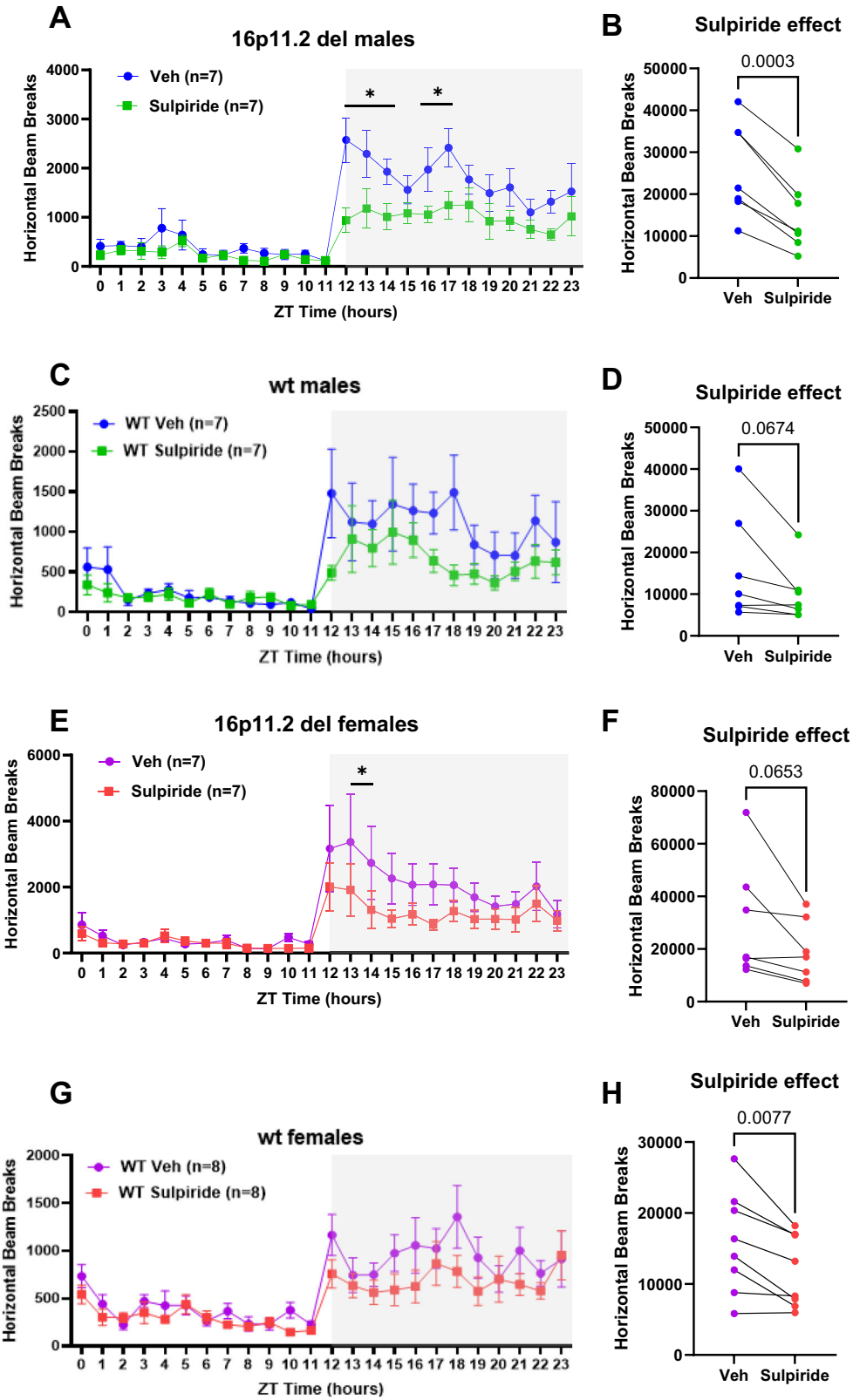

significant polygenic influences, not only in ASD but potentially across a broader spectrum of NDDs, solidifying the 16p11.2 locus as a key source of both common and rare genetic variations[51]. However, previous investigations have failed to pinpoint any single gene within the 16p11.2 locus strongly associated with ASD[52]. Our study delves into the intricate landscape of gene expression in this mutation cell-type specifically. Through single-cell level transcriptomic analysis, we unveil several DEGs within D1- and D2-SPNs associated with ASD based on the SFARI gene database, suggesting a potential compensatory mechanism in response to the mutation. The acquisition of additional genetic hits in the ASD risk genes could predispose carriers to illness, potentially elucidating the phenomenon of healthy carriers. This mechanism also provides insights into the pleiotropy observed in CNVs, where carriers exhibit an increased nonspecific risk. In essence, while carriers

Fig. 5 | D2R antagonist treatment reduces hyperactivity in male 16p11 del/+ mice. A, **B** Infrared beam breaks are plotted across the 24-hr in 1-hr bins (**A**) and in 24-hr (**B**). Activity monitoring data displays decreased hyperactivity after sulpiride injection (50 mg/kg, IP) compared to vehicle injection (5% DMSO in saline, IP) in male 16p11.2 del/+ mice ($n = 7$ vehicle, $n = 7$ Sulpiride). Main effect of treatment F (1, 12) = 4.254, $p = 0.0615$ (**A**) and paired t-test shows $p = 0.0003$ (t = 7.573) between vehicle treatment and sulpiride treatment (**B**). **C**, **D** Activity monitoring data after sulpiride injection (50 mg/kg, IP) compared to vehicle injection (5% DMSO in saline, IP) in male wt mice ($n = 7$ vehicle, $n = 7$ Sulpiride). Main effect of treatment F (1, 12) = 1.186, $p = 0.2976$ (**C**) and paired t-test shows $p = 0.0674$ (t = 2.229) between vehicle treatment and sulpiride treatment (**D**). **E**, **F** In female 16p11.2 del/+ mice ($n = 7$ vehicle, $n = 7$ Sulpiride), main effect of treatment F (1, 12) = 1.416, $p = 0.2570$ (**E**) and paired t-test shows $p = 0.0653$ (t = 2.251) between vehicle treatment and sulpiride treatment (**F**). **G**, **H** In female wt mice ($n = 8$ vehicle, $n = 8$ Sulpiride), main effect of treatment F (1, 12) = 1.656, $p = 0.2191$ (**G**) and paired t-test shows $p = 0.0077$ (t = 3.700) between vehicle treatment and sulpiride treatment (**H**). Source data are provided as a Source Data file for panels A-H.

of CNVs may initially appear healthy due to compensatory mechanisms, the accumulation of additional mutations heightens their susceptibility to diverse disorders, ultimately leading to clinical manifestations. In this context, our snRNA-seq analysis contributes to the growing body of literature elucidating the polygenic effects of ASD risk genes, providing a comprehensive framework for unraveling the complex genetic underpinnings of NDDs. However, our current transcriptional analysis sampled SPNs from both the dorsal and ventral striatum, which encompass functionally and transcriptionally distinct regions. The dorsal striatum and the NAc receive unique inputs and serve different behavioral functions, and prior studies have demonstrated their distinct transcriptional profiles[53]. Given the functional localization of the 16p11.2 deletion effects to the DLS in males, and the potential influence of regional heterogeneity, future studies targeting SPNs within this subregion may be essential for identifying gene candidates underlying altered locomotor behavior.

snRNA-seq analysis identifies genetic factors associated with hyperactive behavior of 16p11.2 del/+ male mice. In our study, single-cell level transcriptomic analysis reveals a substantially different impact of 16p11.2 del/+ on D1- and D2-SPNs. Interestingly, pathway analysis of snRNA-seq reveals that DEGs in both D1- and D2-SPNs are associated with adult locomotory behavior. However, only 16p11.2 del/+ in D2-SPNs mediates hyperactive behaviors. In D2-SPNs, we identify several DEGs that are enriched in the adult locomotory behavior-related pathways and other genes associated with motor regulation or movement deficits. Specifically, *Pde1b*, highly expressed in the striatum and involved in baseline motor activity[54], is upregulated in D2-SPNs in 16p11.2 del/+ mice, indicating a potential molecular mechanism driving hyperactivity. Furthermore, *Atxn2* and *Mtcl2* are associated with motor deficits[55,56]. In addition, comparisons between ASD risk genes and DEGs in D1- or D2-SPNs reveal that 30 DEGs are enriched in 16p11.2 del/+ male mice. Of these, 7 genes (*Adcy5, Camk2b, Herc1, Grin2b, Ube3a, Lrp1*, and *Elavl3*) have been reported to be associated with motor function[29–35]. All seven of these genes show differential expression in D2-SPNs, with four also differentially expressed in both D1- and D2-SPNs. Genes identified in the adult locomotory behavior-related pathway in D2-SPNs, as indicated by GO enrichment network analysis, along with genes enriched in the SFARI gene database, underscore the multifaceted influence of these genetic factors on motor function. Interestingly, this broad effect of 16p11.2 deletion on the expression of a significant number of autism-associated genes potentially serves as an explanation for the polygenic nature of autism and suggests that the study of single locus mutations might reveal a polygenic impact. Moreover, most SFARI-listed ASD risk genes (17 of 21) are upregulated in both D1- and D2-SPNs of 16p11.2 del/+ males, suggesting a potential compensatory response to the mutation. Therefore, investigating the circuit-specific impact of these genes in the striatum will be crucial for future studies, enhancing our understanding of potential mechanisms for hyperactive locomotion.

Our snRNA-seq analysis reveals sex-specific impacts of 16p11.2 del/+ in D1- and D2-SPNs, demonstrating a substantial number of DEGs in males compared to females. Interestingly, gene expression changes in 16p11.2 del/+ males show a significant positive correlation with genes that are more highly expressed in wt females, suggesting a shift in the male transcriptomic profile toward a more female-like state. This observation extends beyond SPNs, as similar patterns were found in bulk striatal RNA-seq data from an independent dataset, indicating that this shift may be a broader striatal phenomenon. One interpretation is that the shift reflects a compensatory transcriptional response in 16p11.2 del/+ males, aligning their gene expression with that of wt females, which may possess protective molecular programs at baseline. Bulk striatal RNA-seq analysis reveals that the genes elevated in wt females and 16p11.2 del/+ males compared to wt males are largely not upregulated in 16p11.2 del/+ females, supporting the hypothesis of male-specific compensation. Our single-cell transcriptomic analysis supports this idea, showing increased expression of several SFARI-listed ASD risk genes in 16p11.2 del/+ males. This raises the possibility that wt females constitutively express protective gene programs, whereas males induce similar compensation only under genetic stress. If additional genetic or environmental risk factors are present, these compensatory mechanisms may become insufficient, ultimately contributing to disease manifestation in humans. These findings raise important questions about how sexual dimorphism in striatal gene regulation interacts with NDD-linked genetic variants. Physiologically, striatal networks differ between sexes, as evidenced by sexual dimorphism in the development of striatal circuits in healthy youth, particularly within cortico-striatal-thalamic circuits[57]. Furthermore, rodent studies have reported sexual dimorphism in neurotransmission, neuronal excitability, and quantity of neuronal subtypes participating in these circuits[58]. Additionally, RiboTag RNAseq studies have highlighted molecular-level sex differences in the striatum, demonstrating moderate sexual dimorphism in D1- and D2-SPNs at baseline[59]. Despite several studies demonstrating sexual dimorphism in NDDs, the understanding of how baseline sexual dimorphism interacts with genetic variation linked to NDDs, leading to sex-specific behavioral phenotypes, is still incomplete. We believe our findings provide a new perspective on the factors influencing male vulnerability or female resilience to NDDs by connecting molecular sexual dimorphism to sex-specific transcriptomic changes and may alert others to consider baseline sex differences more closely in their research. We acknowledge that DEG analysis in snRNA-seq with only two animals per group is limited and should be interpreted with caution. Although similar patterns in bulk striatal RNA-seq provide supporting evidence, confirmation with larger cohorts and independent replication at the single-nucleus level, particularly for D1- and D2-specific patterns, is needed.

In alignment with our observed cell type-specific transcriptomic changes, acute slice electrophysiology experiments reveal a sex- and cell type-specific impairment in inhibitory synaptic transmission in 16p11.2 del/+ mice. Specifically, in D2-SPNs of male 16p11.2 del/+ mice, we observed a reduction in sIPSC frequency in the dorsal striatum and mIPSC frequency in the NAc. Combined with reduced calcium event frequency in D2-SPNs of the dorsal striatum, where hyperactivity emerges, these findings suggest that the mutation leads to D2-SPN hypoactivity, a hallmark of indirect pathway dysfunction. The decreased sIPSC frequency likely reflects reduced engagement of local inhibitory microcircuits, potentially due to diminished D2-SPN firing and weakened reciprocal connectivity. These results appear to contrast with prior reports of elevated sEPSC frequency onto D2-SPNs in 16p11.2 del/+ mice[28], which would typically predict increased calcium

https://doi.org/10.1038/s41467-025-68047-y

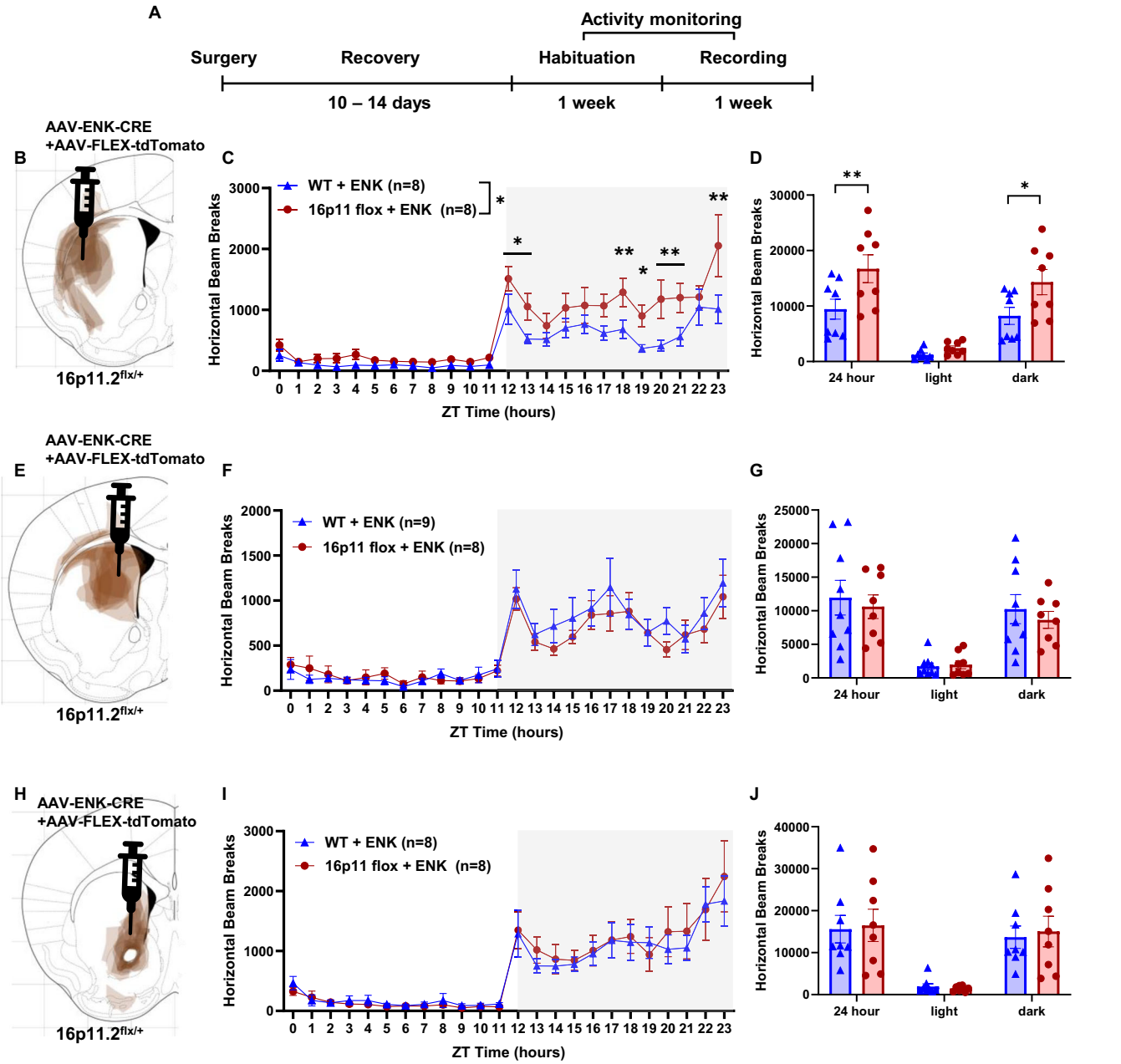

Fig. 6 | 16p11.2 del/+ in D2-SPNs in the dorsal lateral striatum induces hyperactive behavior in males. A Schematic of virus injection and behavioral task timelines. **B** Schematic drawing of virus expression in the dorsal lateral striatum across experiments in the current study ($n = 8$). Red area represents the approximate virus expression. The position of the coronal section is 0.62 mm anterior to Bregma based on the mouse brain atlas[70]. **C** Main effect of genotype, $F(1, 14) = 5.577$, $p = 0.033$; main effect of time, $F(23, 322) = 21.07$, $p < 0.001$; genotype x time interaction, $F(23, 322) = 1.951$, $p < 0.01$. Post hoc shows significant differences between DLS AAV-ENK-CRE injected 16p11.2 flox mice and control littermates in several time slots including 12-13, 18-21, and 23. **D** 24-h plot and dark cycle plot show increased activity in DLS AAV-ENK-CRE injected 16p11.2 flox mice (24-h plot, $t = 3.032$, $p = 0.0041$; dark cycle plot, $t = 2.533$, $p = 0.0151$; $n = 8$ WT, $n = 8$ 16p11.2 flox). **E** Schematic drawing of virus expression (red) in the dorsal medial striatum across experiments in the current study ($n = 7$, 0.62 mm anterior to Bregma based on the mouse brain atlas[70]). **F** Main effect of genotype, $F(1, 15) = 0.1754$, $p = 0.6813$; main effect of time, $F(23, 345) = 24.20$, $p < 0.001$; genotype x time interaction, $F(23, 345) = 0.7224$, $p = 0.8229$. **G** No change is detected in post hoc ($n = 9$ WT, $n = 8$ 16p11.2 flox). **H** Schematic drawing of virus expression (red) in the NAc across experiments in the current study ($n = 7$). The position of the section is 1.18 mm anterior to Bregma based on the mouse brain atlas[70]. (**I**) Main effect of genotype, $F(1, 14) = 0.0317$, $p = 0.8613$; main effect of time, $F(23, 322) = 23.55$, $p < 0.001$; genotype x time interaction, $F(23, 322) = 0.3469$, $p = 0.9981$. (**J**) No change is detected in post hoc ($n = 8$ WT, $n = 8$ 16p11.2 flox). Error bars represent SEM. $^*p < 0.05$, $^{**}p < 0.01$. Source data are provided as a Source Data file for (**C**, **D**, **F**, **G**, **I**, **J**).

activity. This discrepancy may reflect compensatory mechanisms that reduce firing or calcium signaling downstream of excitatory synaptic input in the slice preparation. It may also reflect region-specific effects, as the sEPSC data were from the NAc. Together, these findings reveal a region- and sex-specific disruption of inhibitory signaling, with D2-SPNs in 16p11.2 del/+ males showing selective vulnerability. This impairment of local inhibition may represent a key circuit mechanism underlying the observed behavioral alterations, such as ASD and ADHD.

In conclusion, this study demonstrates that a CNV associated with NDDs acts in distinct ways in different neuronal circuits, impacting gene expression, synaptic function, and behavior in a sex-specific

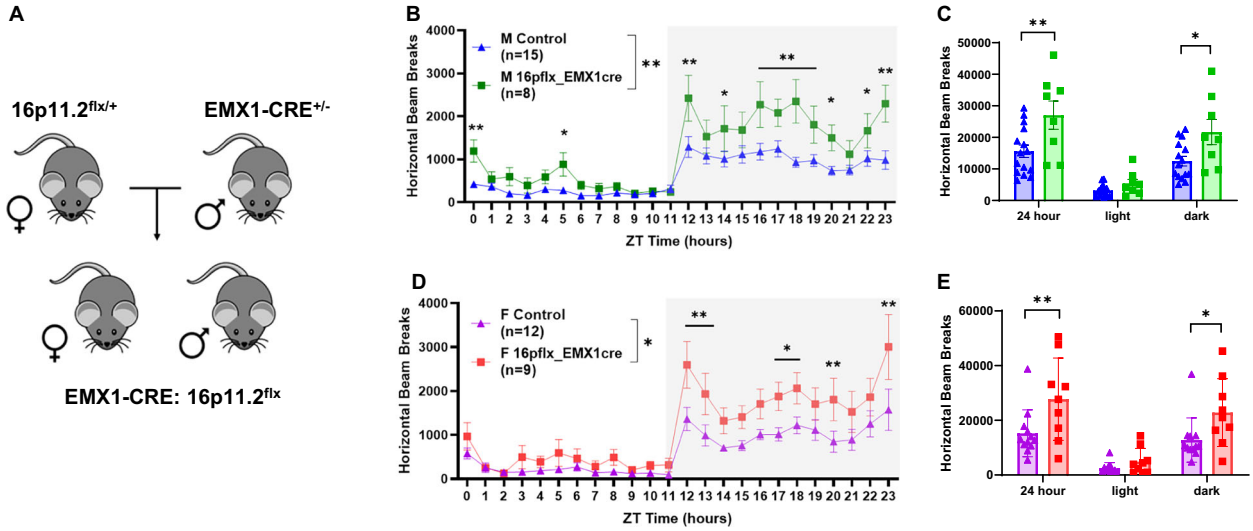

Fig. 7 | Cortex-specific 16p11.2 del/+ drives hyperactive behavior in both sexes. **A** Genetic crosses used to induce 16p11.2 del/+ in the cortex. **B**, **C** Activity monitoring shows increased activity in male EMX1-CRE x 16p11.2 flox mice. **B** Main effect of genotype, $F(1, 21) = 9.199$, $p = 0.0063$; main effect of time, $F(23, 483) = 24.20$, $p < 0.001$; genotype x time interaction, $F(23, 483) = 2.984$, $p < 0.001$). Post hoc shows significant differences between male EMX1-CRE x 16p11.2 flox mice and control littermates in several time slots. (**C**) 24-hour plot ($t = 3.524$, $p = 0.0024$) and dark plot ($t = 2.834$, $p = 0.0185$) show increased activity in male EMX1-CRE x 16p11.2 flox mice ($n = 15$ control, $n = 8$ Ctx-16p11.2 del). **D**, **E** Female EMX1-CRE x 16p11.2 flox mice show hyperactivity compared to control littermates. **D** Main effect of genotype, $F(1, 19) = 5.815$, $p = 0.0262$; main effect of time, $F(23, 437) = 20.81$, $p < 0.001$; genotype x time interaction, $F(23, 437) = 1.785$, $p = 0.0147$). Post hoc shows hyperactivity of female EMX1-CRE x 16p11.2 flox mice in several time slots. **E** 24-h plot ($t = 3.083$, $p = 0.0095$) and dark plot ($t = 2.487$, $p = 0.0475$) show increased activity in female EMX1-CRE x 16p11.2 flox mice ($n = 12$ control, $n = 9$ Ctx-16p11.2 del). Error bars represent SEM. Source data are provided as a Source Data file for (**B**–**E**).

fashion. These findings provide new insight into male vulnerability or female resilience to NDDs, highlighting striatal circuits as key mediators of symptoms of NDDs and offering new avenues for circuit-based, sex-specific therapeutic approaches.

Methods

Animals

Mice were housed (2–5 per cage) in a room maintained on a 12-h light/dark cycle (20–25 °C, 30–70% humidity) with *ad libitum* access to food and water. All procedures were approved by the University of Iowa Institutional Animal Care and Use Committee, and followed policies set forth by the National Institutes of Health Guide for the Care and Use of Laboratory Animals. 16p11.2 del/+ mice were produced by breeding male B6129S-Del(7Slx1b-Sept1)4Aam/J mice purchased from The Jackson Laboratory (Stock #013128) with female B6129SF1/J mice (Stock #101043), as previously described[25]. The 593 kb CNV (chr6, 133.84-134.28 Mb) conditioned mouse line was generated in the Mills laboratory to delete the causative region in specific neurons of the developing brain using chromosome engineering[60]. This conditional model has a floxed version of the region analogous to 16p11.2, and when crossed to a cell-type specific CRE mouse model, causes efficient deletion of the floxed region in vivo[61]. To generate mice with cell type-specific deletion of the region analogous to 16p11.2 (the 7F4 region in mice) specifically in D1- or D2-SPNs, we used the EY217 Drd1a-CRE line (purchased from GENSAT, B6.FVB(Cg)-Tg(Drd1a-re)EY217Gsat/Mmucd, Stock Number :034258-UCD) and KG139 A2A-CRE line (purchased from GENSAT, B6.FVB(Cg)-Tg(Adora2a-CRE)KG139Gsat/Mmucd, Stock Number 036158-UCD). These CRE lines were backcrossed at least 5 generations to 129S1 (purchased from The Jackson Laboratory, 129S1/SvImJ, Stock Number 002448) and bred to floxed 16p11.2 hemizygous mice created by our collaborator Alea Mills at Cold Spring Harbor Laboratory[60]. To selectively introduce the 16p11.2 del/+ in the cortex, we used the Emx1-CRE line (purchased from The Jackson Laboratory, B6.129S2-Emx1tm1(CRE) Krj/J, Stock Number 005628). Emx1-CRE mice express the CRE recombinase in cortical excitatory neurons and glia, but not GABAergic neurons[62]. To selectively introduce the 16p11.2 del/+ in D2-SPNs, we utilized A2a-CRE mice instead of D2-CRE mice because CRE recombinase is expressed in striatal cholinergic interneurons as well as D2-SPNs of D2-CRE mice[63], unlike A2a-CRE mice, which drives expression in D2-SPNs but not cholinergic interneurons[18]. Experimental data was collected from littermate animals during the same time period. Mice aged between 10 and 16 weeks were randomly used for experiments to minimize any bias unless otherwise specified.

Genotyping. PCR-genotyping was done to identify founders with the intended mutation.

16p11.2 del/+
wt Fwd GCTATGAAGATGCCCACCAT
wt Rev GTGGTAACTCATGCGGTCCT
mut Fwd CAAGCACTGGCTATGCATGT
mut Rev AAGACAGAATGCTATGCAACCTT
sD1-CRE
Drd1a Fwd GCTATGGAGATGCTCCTGATGGAA
CreGS Rev CGGCAAACGGACAGAAGCATT
A2A-CRE
Adora2a Fwd CGTGAGAAAGCCTTTGGGAAGCT
CreGS Rev CGGCAAACGGACAGAAGCATT
EMX1-CRE
Common Fwd CAACGGGGAGGACATTGA
wt Rev CAAAGACAGAGACATGGAGAGC
mu Rev TCGATAAGCCAGGGGTTC
16p11.2 flox
#1672 (SF 5′ Vector S1) GCGCCCAATACGCAAACCGCC
#1673 (SF 216K12 gap For/Compl) TCCTCCACTGCTGGTAGGAG
#1674 (SF 135K15AFEO gap1 REV) GCATGTGTGCACTAACCTA TATCC
#1675 (SF 3′ Vector S1) TGCGGGCCTCTTCGCTATTACG
16p11.2 df allele
df FwdCCTCATGGACTAATTATGGAC
df RevCCAGTTTCACTAATGACACA

Single-cell RNA-sequencing

Tissue processing for scRNA-seq. Mice were sacrificed at 14-16 weeks of age by live decapitation and the brain was rapidly removed. Using a mouse brain matrix, 1 mm coronal sections were collected, and then tissue punches containing the striatum (-0.5 ~ 1.5 mm AP from bregma; n = 2 mice/genotype/sex) were rapidly frozen on dry ice. Tissue punches were preserved at -80 °C until the day of single nuclei dissociation. Each snRNA-seq experimental set consisted of male wt, male 16p11.2 del/+, female wt, and female 16p11.2 del/+ littermates. Animals were selected from two separate litters originating from different breeding cages.

Single nuclei purification. For single nuclei dissociation, a protocol from a previous study was followed[64]. Briefly, frozen tissue punches were chopped and transferred to 450 µl of chilled (4 °C) homogenization buffer (250 mM sucrose, 25 mM KCl, 5 mM $MgCl_2$, 10 mM Tris buffer (pH 8.0), 1 µM DTT, 1x protease inhibitor, RNaseIn 0.4 U/µl, SUPERase-In 0.2 U/µl, 0.1% Triton X-100). After the Dounce homogenization and filtering (40µm), the nuclei were concentrated by centrifugation (1,000 g for 8 min at 4 °C). For staining, anti-NeuN antibody (Millipore MAB377, 1:500), Hoechst, and Alexa 488 secondary antibody (Invitrogen A32723, 1:500) were treated and incubated on a rocker in a cold room for 30 min. The nuclei were resuspended in 600 µl FACS buffer (1% unacetylated BSA, RNaseIn 0.4 U/µl, PBS) for FACS to further purify the nuclei for sequencing. The nuclei were first sorted based on Hoechst signal and then based on Alexa 488 fluorophore, collecting 50,000 nuclei per mouse.

Single nuclear (snRNA) RNA sequencing and analysis. Libraries were constructed using the 3′ Expression-Single-Cell RNA-Seq using 10X Chromium System (v3.1), according to the manufacturer's instructions. The nuclei were brought to a concentration of 500 nuclei/µl and 5000 nuclei were loaded to prepare libraries. Libraries were then sequenced (pair-end sequencing) on the Illumina NovaSeq6000 at the Iowa Institute of Human Genetics at the University of Iowa. The depth of sequencing per flow cell was 50,000 reads per nuclei. FASTQ files were aligned to the pre-mRNA annotated *Mus musculus* reference genome version GRCm38 (refdata-cellranger-mm10-3.0.0). Cell Ranger Count v3.0.2 (10x Genomics, Pleasanton CA) was used on FASTQ data from each of the GEM wells individually for genome alignment and feature-barcode matrix counts generation. Cell Ranger Aggr v3.0.2 was then used to combine data from multiple samples of the same genotype (biological replicates) into an experiment-wide feature-barcode matrix and analysis, normalize those runs to the same sequencing depth, and then recompute the feature-barcode matrices and analysis on the combined data. This raw expression Unique Molecular Identifiers (UMI) counts matrix contains cells as rows and genes as columns and can be further used for downstream analysis such as normalization, clustering, differentially expressed genes, etc.

The clusters were then visualized with uniform manifold approximation and projection (UMAP) in two dimensions of UMI per cells (figure S1). The most significant gene markers corresponding to each cluster and conserved across the two genotypes (WT and 16p11.2 del/+) were used to identify the cell-types by correlating with previously published single-cell data[65] and from the transcriptomic explorer of the Allen Brain Atlas (https://celltypes.brain-map.org/rnaseq/mouse_ctx-hip_10x). To obtain an observer-independent data-driven characterization of cell types, we computed the 2000 most variable genes in each cell, based on the assumption that these genes will distinguish best between different cell types and formed clusters of specific cell types based on similar transcriptomic signatures for each cell (Fig. 1B, S1, S2). DotPlot representations show the normalized UMI expression of conserved gene markers across the two genotypes in the different cell types.

Raw single nuclei RNA-seq UMI count data was used for clustering analysis using the Seurat R analysis pipeline[66]. First, cells with more than 50,000 molecules (nUMI per cell) were filtered out to discard potential doublets. Post filtering, the raw UMI counts from the primary filtered dataset were used for log-normalization and scaled using a factor of 10,000 and regressed to covariates such as number as described in the Seurat analysis pipeline[66]. To further identify the top variable genes, the data was used to calculate principal components (PCs). Using Jackstraw analysis, statistically significant PCs were used to identify clusters within the data using original Louvain algorithm as described in the Seurat analysis pipeline, followed by visualizing the clusters with uniform manifold approximation and projection (UMAP) in two dimensions of UMI per cells[67]. Genes corresponding to each cluster were used to identify the cell-type by correlating to genes expressed in previously published adult mouse striatal single-cell data[65] and analyzed for expression of top marker genes of known cell types.

Pairwise differential gene expression analysis tests were performed within each cluster-pair (wt vs. 16p11.2 del/+) using a Wilcoxon Rank Sum test (a two-sided test, with Benjamini–Hochberg correction to control the false discovery rate) from the Seurat R analysis pipeline[66] to identify differentially expressed genes. Genes with an adjusted p-value under 0.05 and an absolute $\log_2$ fold change above 0.2 were considered significantly differentially expressed. Enrichment analysis of DEG-associated pathways and molecular functions from snRNA-seq was performed with a combination of Kyoto Encyclopedia of Genes and Genomes (KEGG) and the Gene Ontology (GO-Molecular Function-EBI-Uniport-GOA-) databases. The analyses were done with Cytoscape (version.3.8.0, https://cytoscape.org/)[68] plug-in ClueGO (version 2.5.6)[69]. Only the pathways with a p-value < 0.05 and gene counts ≥ 3 were considered as significant and displayed. To connect the terms in the network, ClueGO utilizes kappa statistics which was set as ≥ 0.4.

Electrophysiology

Virus Injection and stereotaxic injections. For the cell-type–specific electrophysiology approach, we used AAV-ENK-CRE and AAV-PPTA-CRE viruses, kindly provided by Dr. Jocelyne Caboche (Sorbonne University). AAV-ENK-CRE targets D2-SPNs, and AAV-PPTA-CRE targets D1-SPNs, each driving CRE recombinase expression in those specific neurons[36,37]. pAAV-FLEX-tdTomato and pAAV-FLEX-GFP viruses (purchased from Addgene; catalog numbers 28306 and 28304, respectively) were used in combination with AAV-ENK-CRE or AAV-PPTA-CRE. 16p11.2 del/+ mice were injected with the virus mixture—10^{12} vg/animal for AAV-ENK-CRE and 1×10^{11} vg/animal for pAAV-FLEX-tdTomato, or 10^{12} vg/animal for AAV-PPTA-CRE and 1×10^{11} vg/animal for pAAV-FLEX-GFP—into each hemisphere of the dorsal striatum (AP: +0.65 mm; ML: ±2.00 mm; DV: −3.2 mm from bregma). The rate of injection was 200 nl/min with a total volume of 1 µl per striatum. Injections were performed at ~2–3 months of age. Mice were prepared for recordings following 2–3 weeks of viral expression.

Brain slice preparation. Mice were decapitated, and brains were excised rapidly between zeitgeber time (ZT) 2 and ZT 4, relative to lights-off at ZT 12. Coronal brain slices 300-µm-thick were prepared using a Leica VT1200S (Leica Biosystems) vibrating blade microtome. During the brain slice preparation, the brain was immersed in an ice-cold, oxygenated (95% O_2, 5% CO_2) sucrose solution containing the following (in mM): 75.1 sucrose, 75 NaCl, 2.5 KCl, 1.2 NaH_2PO_4, 30 $NaHCO_3$, 20 HEPES, 25 glucose, 10 $MgSO_4$ and 0.5 $CaCl_2$. After slicing, the slices were immediately incubated in oxygenated artificial cerebrospinal fluid (ACSF) containing the following (in mM): 92 NaCl, 2.5 KCl, 1.2 NaH_2PO_4, 30 $NaHCO_3$, 20 HEPES, 25 glucose, 2 $MgSO_4$ and 2 $CaCl_2$, for 30 min and transferred to room temperature for a minimum of 30 min. Osmolarity of the solutions was kept between 298-300 mOsm.

Electrophysiological recording conditions and data acquisition. Slices were individually transferred to a recording chamber on the stage

of an upright BX51WI microscope. The recording ACSF (containing the following (in mM): 124 NaCl, 2.5 KCl, 1.2 NaH_2PO_4, 24 $NaHCO_3$, 5 HEPES, 12.5 glucose, 1.3 $MgSO_4$ and 2.5 $CaCl_2$) was heated to 28-30 °C using a perfusion temperature controller and circulated at a rate of 1.5 ml/min using a peristaltic pump. Neurons expressing tdTomato/EGFP were identified using a combination of a SciCam Pro camera and fluorescence microscopy connected to a pE-400 illumination system. Data acquisition was done using a dPatch2 amplifier (Sutter Instruments) and Igor Pro 9. The intracellular pipette solution [containing the following (in mM): 130 Cs-methane sulfonate, 8 CsCl, 10 HEPES, 0.6 EGTA, 1 $MgCl_2$, 5 QX-314 and 0.1 spermine; osmolarity ~ 290-295 mOsm] was prepared and adjusted to a pH of 7.2 using CsOH. The current signals were acquired at 20 kHz and filtered at 4 kHz. Series resistance (R_s) was monitored using an access test analyzing the membrane current response to multiple 20 msec, 5 mV hyperpolarizing voltage steps from −65 mV. The access test was performed before and after each recording, and only cells with R_s < 20 MΩ and R_s change during the recording <20% were used for subsequent analysis. Spontaneous inhibitory postsynaptic currents (sIPSCs) were pharmacologically isolated by using 50 μM D-APV and 20 μM NBQX and recorded at +10 mV.

Analysis. sIPSC analysis was done using custom Python scripts developed to extract and process the electrophysiological recordings stored in HDF5 (.h5) format and the metadata in notebook files. A minimum of 150 individual events per cell were included for analysis to ensure reliable estimation of synaptic parameters. Event detection used the scipy function find_peaks, applied to traces that were lowpass filtered using a 4 pole butterworth filter with cutoff of 1000 Hz, and with prominence parameter of 15 pA, width parameter of 5 ms, and wlen parameter of 0.1. All the custom codes used for event detection, extraction, and synaptic parameter analysis are available from the GitHub repository: (https://github.com/neurord/ephys_anal/releases/tag/v2.0).

Fiber photometry and surgeries

Mice were injected with AAV-syn-jGCaMP7f-WPRE (10^{13} vg/mL, AAV9 #104488, Addgene) into the dorsal striatum (AP: +0.65 mm; ML: ±2.0 mm; DV: −3.2 mm from bregma). The injection rate was 200 nL/min, with a total volume of 1 μL per hemisphere. For cell type-specific fiber photometry recordings, mice were co-injected with AAV-PPTA-CRE (10^{12} vg/mL) or AAV-ENK-CRE (10^{12} vg/mL) and AAV-syn-FLEX-jGCaMP8m-WPRE (10^{13} vg/mL, AAV9 #162378, Addgene). A 200-μm core, 1.25-mm ferrule, 0.37-NA optical fiber (Neurophotometrics) was implanted at the same location (AP: +0.65 mm; ML: ±2.0 mm; DV: −3.0 mm from bregma) and secured with dental cement. Following two weeks of viral expression, fiber photometry recordings were performed using the FP3002 system (Neurophotometrics) and recorded with Bonsai software for 2–3 min in the homecage. Two LED wavelengths were used: 415 nm (isosbestic control) and 470 nm (GCaMP excitation). GCaMP fluorescence signals were analyzed using MATLAB scripts adapted from the Neurophotometrics Data Analysis Manual. To calculate the percentage change in fluorescence (%ΔF/F), the isosbestic signal was first fitted with a biexponential decay curve. This fit was scaled to the calcium-dependent signal, which was then divided by the scaled fit. The %ΔF/F was computed using the fitted isosbestic signal (F) and the calcium-dependent signal (ΔF). Instantaneous spike frequency was estimated using spike detection MATLAB scripts (minimum peak prominence of 1), also adapted from the Neurophotometrics Data Analysis Manual.

Activity monitoring

An infrared beam-break system (Opto M3, Columbus Instruments, Columbus, OH) was used to measure mice locomotor activity, as previously described[26]. Behavior experiments were designed based on previous experience with an effect size of 0.7 in a power analysis. The mice were acclimatized to the monitoring chambers for one week before data collection to reduce the effect of a new environment. The data was collected for one week following the habituation period. ANOVAs followed by Fisher's LSD post-hoc tests were performed using GraphPad 9 (La Jolla, CA), with genotype as the between-subjects factor and time as the within-subjects factor, as previously described[26]. After behavioral assessments, the striatum and adjacent cortices were dissected from D1- and D2-16p11.2 del/+ and control mice to confirm the hemideletion of the 16p11.2 region in the striatum using PCR (figure S12).

Drug treatment

For intraperitoneal injections (IP), sulpiride (50 mg/kg in a volume of 5 ml/kg, Sigma-Aldrich, Product No. S8010) was dissolved in 0.9% saline, 5% DMSO, and 1% acetic acid which was then neutralized using NaOH to pH7. Vehicle treatment received 5 ml/kg of 5% DMSO in saline. The mice were acclimatized to the monitoring chambers for one week before data collection to reduce the effect of a new environment. In the second week, mice were injected with vehicle daily at the beginning of the dark cycle (total of 7 vehicle injections). In the third week, mice were injected with sulpiride at the beginning of the dark cycle everyday (total of 7 drug injections). The data was collected for two weeks following the habituation period. The effect size was determined using Cohen's $d = (M2-M1)/SD_{pooled}$, where $SDpooled = \sqrt{((SD1^2 + SD2^2)/2)}$.

Virus Injection and stereotaxic injections

16p11.2 flox mice were injected with the virus mix (10^{12} vg/animal for AAV-ENK-CRE and 1×10^{11} vg/animal for either pAAV-FLEX-tdTomato and pAAV-FLEX-GFP) into the dorsal medial striatum (AP, +0.65 mm; ML, ± 1.70 mm; DV, -3.2 mm from bregma), dorsal lateral striatum (AP, +0.65 mm; ML, ± 2.2 mm; DV, -3.2 mm from bregma) or NAc (AP, +1.2 mm; ML, ±1.0 mm; DV, -4.2 mm from bregma). The rate of injection was 200 nl/min with a total volume of 1 μl per striatum. Following 2 weeks of virus expression, mice were tested in activity monitoring. After behavioral assessments, the striatum and cerebellum were dissected from 16p11.2 flox and control mice to confirm the hemideletion of the 16p11.2 region using PCR (figure S13).

Fluorescence imaging

After activity monitoring, mice were cervically dislocated and decapitated, and the whole brain removed on ice. Brain tissue was immersed in the 4% formaldehyde (PFA) at 4 °C overnight. The tissue was transferred into 30% sucrose for 48 h. Then, tissue was sliced into 40 μm thick sections using a cryostat at -20 °C and mounted on slides. Fluorescence images were taken with a Leica DM6B Upright digital microscope using the software program NeuroLucida (Microbrightfield Inc). Placements were identified with reference to a mouse brain atlas[70].

Reporting summary

Further information on research design is available in the Nature Portfolio Reporting Summary linked to this article.

Data availability

The snRNAseq datasets generated and/or analyzed during the current study are available in the NCBI's Gene Expression Omnibus repository, GEO Series accession GSE266222 [GEO Accession viewer], and Figshare (https://doi.org/10.6084/m9.figshare.25723917). The whole cell recording data and behavioral data generated in this study are provided in the Supplementary Information/Source Data file. Source data are provided with this paper.

Code availability

The code for analyses and figures related to snRNA-seq data can be accessed through GitHub - YannVRB/snRNA-seq-16p11.2-del-males-females and YannVRB/snRNA-seq-16p11.2-del-males-females: v1.0.0

(https://doi.org/10.5281/zenodo.17601371). Files used to analyze whole cell recording data can be accessed through Release Jaekyoon Kim et al. 2025 · neurord/ephys_anal · GitHub and neurord/ephys_anal: Jaekyoon Kim et al. 2025 (https://doi.org/10.5281/zenodo.17584161).

References

1. Bolte, S. et al. Sex and gender in neurodevelopmental conditions. *Nat. Rev. Neurol.* **19**, 136–159 (2023).
2. Vegeto, E. et al. The Role of Sex and Sex Hormones in Neurodegenerative Diseases. *Endocr. Rev.* **41**, 273–319 (2020).
3. Ostrom, Q. T. et al. Risk factors for childhood and adult primary brain tumors. *Neuro Oncol.* **21**, 1357–1375 (2019).
4. Rubinow, D. R. & Schmidt, P. J. Sex differences and the neurobiology of affective disorders. *Neuropsychopharmacology* **44**, 111–128 (2019).
5. Faheem, M. et al. Gender-based differences in prevalence and effects of ADHD in adults: a systematic review. *Asian J. Psychiatr.* **75**, 103205 (2022).
6. Ferri, S. L., Abel, T. & Brodkin, E. S. Sex differences in autism spectrum disorder: a review. *Curr. Psychiatry Rep.* **20**, 9 (2018).
7. Halladay, A. K. et al. Sex and gender differences in autism spectrum disorder: summarizing evidence gaps and identifying emerging areas of priority. *Mol. Autism* **6**, 36 (2015).
8. Mandy, W. et al. Sex differences in autism spectrum disorder: evidence from a large sample of children and adolescents. *J. Autism Dev. Disord.* **42**, 1304–1313 (2012).
9. McCarthy, M. M. & Arnold, A. P. Reframing sexual differentiation of the brain. *Nat. Neurosci.* **14**, 677–683 (2011).
10. McCarthy, M. M. A new view of sexual differentiation of mammalian brain. *J. Comp. Physiol.* **206**, 369–378 (2020).
11. Fuccillo, M. V. Striatal circuits as a common node for autism pathophysiology. *Front. Neurosci.* **10**, 27 (2016).
12. Nickl-Jockschat, T. et al. Brain structure anomalies in autism spectrum disorder–a meta-analysis of VBM studies using anatomic likelihood estimation. *Hum. Brain Mapp.* **33**, 1470–1489 (2012).
13. Langen, M. et al. Changes in the development of striatum are involved in repetitive behavior in autism. *Biol. Psychiatry* **76**, 405–411 (2014).
14. Evans, M. M., Kim, J., Abel, T., Nickl-Jockschat, T. & Stevens, H. E. Developmental disruptions of the dorsal striatum in autism spectrum disorder. *Biol. Psychiatry* **95**, 102–111 (2024).
15. Graybiel, A. M., Aosaki, T., Flaherty, A. W. & Kimura, M. The Basal Ganglia and Adaptive Motor Control. *Science* **265**, 1826–1831 (1994).
16. Carlsson, L. H. et al. Coexisting disorders and problems in preschool children with autism spectrum disorders. *ScientificWorldJournal* **2013**, 213979 (2013).
17. Kravitz, A. V. et al. Regulation of parkinsonian motor behaviours by optogenetic control of basal ganglia circuitry. *Nature* **466**, 622–626 (2010).
18. Durieux, P. F. et al. D2R striatopallidal neurons inhibit both locomotor and drug reward processes. *Nat. Neurosci.* **12**, 393–395 (2009).
19. Krajeski, R. N., Macey-Dare, A., van Heusden, F., Ebrahimjee, F. & Ellender, T. J. Dynamic postnatal development of the cellular and circuit properties of striatal D1 and D2 spiny projection neurons. *J. Physiol.* **597**, 5265–5293 (2019).
20. Hanson, E. et al. The cognitive and behavioral phenotype of the 16p11.2 deletion in a clinically ascertained population. *Biol. Psychiatry* **77**, 785–793 (2015).
21. Rein, B. & Yan, Z. 16p11.2 Copy number variations and neurodevelopmental disorders. *Trends Neurosci.* **43**, 886–901 (2020).
22. Weiss, L. A. et al. Association between microdeletion and microduplication at 16p11. 2 and autism. *N. Engl. J. Med.* **358**, 667–675 (2008).
23. Rosenfeld, J. A. et al. Copy number variations associated with autism spectrum disorders contribute to a spectrum of neurodevelopmental disorders. *Genet. Med.* **12**, 694–702 (2010).
24. Hudac, C. M. et al. Evaluating heterogeneity in ASD symptomatology, cognitive ability, and adaptive functioning among 16p11.2 CNV carriers. *Autism Res.* **13**, 1300–1310 (2020).
25. Lynch, J. F. et al. Comprehensive behavioral phenotyping of a 16p11.2 del mouse model for neurodevelopmental disorders. *Autism Res.* **13**, 1670–1684 (2020).
26. Angelakos, C. C. et al. Hyperactivity and male-specific sleep deficits in the 16p11.2 deletion mouse model of autism. *Autism Res.* **10**, 572–584 (2017).
27. Grissom, N. M. et al. Male-specific deficits in natural reward learning in a mouse model of neurodevelopmental disorders. *Mol. Psychiatry* **23**, 544–555 (2018).
28. Portmann, T. et al. Behavioral abnormalities and circuit defects in the basal ganglia of a mouse model of 16p11.2 deletion syndrome. *Cell Rep.* **7**, 1077–1092 (2014).
29. Adhikari, A. et al. Functional rescue in an Angelman syndrome model following treatment with lentivector transduced hematopoietic stem cells. *Hum. Mol. Genet.* **30**, 1067–1083 (2021).
30. Carecchio, M. et al. ADCY5-related movement disorders: Frequency, disease course and phenotypic variability in a cohort of paediatric patients. *Parkinsonism Relat. Disord.* **41**, 37–43 (2017).
31. Duan, Y. et al. Striatal GluN2B involved in motor skill learning and stimulus-response learning. *Neuropharmacology* **135**, 73–85 (2018).
32. Kool, M. J., van de Bree, J. E., Bodde, H. E., Elgersma, Y. & van Woerden, G. M. The molecular, temporal and region-specific requirements of the beta isoform of Calcium/Calmodulin-dependent protein kinase type 2 (CAMK2B) in mouse locomotion. *Sci. Rep.* **6**, 26989 (2016).
33. Lalonde, R. & Strazielle, C. The Herc1 gene in neurobiology. *Gene* **814**, 146144 (2022).
34. Ogawa, Y. et al. Elavl3 is essential for the maintenance of Purkinje neuron axons. *Sci. Rep.* **8**, 2722 (2018).
35. May, P. et al. Neuronal LRP1 functionally associates with postsynaptic proteins and is required for normal motor function in mice. *Mol. Cell. Biol.* **24**, 8872–8883 (2004).
36. Lissek, T. et al. Npas4 regulates medium spiny neuron physiology and gates cocaine-induced hyperlocomotion. *EMBO Rep.* **22**, e51882 (2021).
37. Holt, A. G. & Newman, S. W. Distribution of methionine and leucine enkephalin neurons within the social behavior circuitry of the male Syrian hamster brain. *Brain Res* **1030**, 28–48 (2004).
38. Lipton, D. M., Gonzales, B. J. & Citri, A. Dorsal Striatal Circuits for Habits, Compulsions and Addictions. *Front Syst. Neurosci.* **13**, 28 (2019).
39. Munro, C. A. et al. Sex differences in striatal dopamine release in healthy adults. *Biol. Psychiatry* **59**, 966–974 (2006).
40. Brundage, J. N. et al. Regional and sex differences in spontaneous striatal dopamine transmission. *J. Neurochem* **160**, 598–612 (2022).
41. Williams, O.O.F., Coppolino, M., George, S.R., & Perreault, M.L. Sex differences in dopamine receptors and relevance to neuropsychiatric disorders. *Brain Sci.* **11**, 1199 (2021).
42. Cummings, J. A., Jagannathan, L., Jackson, L. R. & Becker, J. B. Sex differences in the effects of estradiol in the nucleus accumbens and striatum on the response to cocaine: neurochemistry and behavior. *Drug Alcohol Depend.* **135**, 22–28 (2014).
43. Van Zandt, M., Flanagan. D. & Pittenger, C. Sex differences in the distribution and density of regulatory interneurons in the striatum. *Front. Cell. Neurosci.* **18**, 1415015 (2024).
44. Weber E.T., Andrade R. Htr2a Gene and 5-HT(2A) receptor expression in the cerebral cortex studied using genetically modified mice. *Front. Neurosci.* **4**, 36 (2010).
45. Foster, N. N. et al. The mouse cortico-basal ganglia-thalamic network. *Nature* **598**, 188–194 (2021).
46. Koketsu, D., Chiken, S., Hisatsune, T., Miyachi, S. & Nambu, A. Elimination of the Cortico-Subthalamic Hyperdirect Pathway

Induces Motor Hyperactivity in Mice. *J. Neurosci.* **41**, 5502–5510 (2021).
47. Cui, G. et al. Concurrent activation of striatal direct and indirect pathways during action initiation. *Nature* **494**, 238–242 (2013).
48. Sheng, M. J., Lu, D., Shen, Z. M. & Poo, M. M. Emergence of stable striatal D1R and D2R neuronal ensembles with distinct firing sequence during motor learning. *Proc. Natl. Acad. Sci. USA* **116**, 11038–11047 (2019).
49. Smith, A. C. W. et al. Opposing roles for striatonigral and striatopallidal neurons in dorsolateral striatum in consolidating new instrumental actions. *Nat. Commun.* **12**, 5121 (2021).
50. Zeighami, Y. et al. A comparison of anatomic and cellular transcriptome structures across 40 human brain diseases. *PLoS Biol.* **21**, e3002058 (2023).
51. Weiner, D. J. et al. Statistical and functional convergence of common and rare genetic influences on autism at chromosome 16p. *Nat. Genet.* **54**, 1630–1639 (2022).
52. Fu, J. M. et al. Rare coding variation provides insight into the genetic architecture and phenotypic context of autism. *Nat. Genet.* **54**, 1320–1331 (2022).
53. Montalban, E. et al. Translational profiling of mouse dopaminoceptive neurons reveals region-specific gene expression, exon usage, and striatal prostaglandin E2 modulatory effects. *Mol. Psychiatry* **27**, 2068–2079 (2022).
54. Siuciak, J. A. et al. Behavioral and neurochemical characterization of mice deficient in the phosphodiesterase-1B (PDE1B) enzyme. *Neuropharmacology* **53**, 113–124 (2007).
55. Crunkhorn, S. Neurodegenerative disorders: Ataxin 2 reduction rescues motor defects. *Nat. Rev. Drug Discov.* **16**, 384–385 (2017).
56. Satake, T. et al. MTCL1 plays an essential role in maintaining Purkinje neuron axon initial segment. *EMBO J.* **36**, 1227–1242 (2017).
57. Jacobs, G. R. et al. Developmentally divergent sexual dimorphism in the cortico-striatal-thalamic-cortical psychosis risk pathway. *Neuropsychopharmacology* **44**, 1649–1658 (2019).
58. Zachry, J. E. et al. Sex differences in dopamine release regulation in the striatum. *Neuropsychopharmacology* **46**, 491–499 (2021).
59. Kronman, H. et al. Biology and Bias in cell type-specific RNAseq of nucleus accumbens medium spiny neurons. *Sci. Rep.* **9**, 8350 (2019).
60. Horev, G. et al. Dosage-dependent phenotypes in models of 16p11.2 lesions found in autism. *P Natl. Acad. Sci. USA* **108**, 17076–17081 (2011).
61. Mills, A. A., Qi, Y. & Bradley, A. Conditional inactivation of p63 by Cre-mediated excision. *Genesis* **32**, 138–141 (2002).
62. Gorski, J. A. et al. Cortical excitatory neurons and glia, but not GABAergic neurons, are produced in the Emx1-expressing lineage. *J. Neurosci.* **22**, 6309–6314 (2002).
63. Durieux, P. F., Schiffmann, S. N. & d'Exaerde, deK. erchove A. Targeting neuronal populations of the striatum. *Front. Neuroanat.* **5**, 40 (2011).
64. Krishnaswami, S. R. et al. Using single nuclei for RNA-seq to capture the transcriptome of postmortem neurons. *Nat. Protoc.* **11**, 499–524 (2016).
65. Saunders, A. et al. Molecular diversity and specializations among the cells of the adult mouse brain. *Cell* **174**, 1015–1030 e1016 (2018).
66. Butler, A., Hoffman, P., Smibert, P., Papalexi, E. & Satija, R. Integrating single-cell transcriptomic data across different conditions, technologies, and species. *Nat. Biotechnol.* **36**, 411–420 (2018).
67. Becht E, et al. Dimensionality reduction for visualizing single-cell data using UMAP. *Nat. Biotechnol.* **37**, 38–44(2018).
68. Shannon, P. et al. Cytoscape: a software environment for integrated models of biomolecular interaction networks. *Genome Res.* **13**, 2498–2504 (2003).
69. Bindea, G. et al. ClueGO: a cytoscape plug-in to decipher functionally grouped gene ontology and pathway annotation networks. *Bioinformatics* **25**, 1091–1093 (2009).
70. Paxinos, G., Franklin, K.B. *The mouse brain in stereotaxic coordinates: compact*. Amsterdam San Diago, CA (2004).

Acknowledgements

This work was supported by The University of Iowa Hawkeye Intellectual and Developmental Disabilities Research Center (HAWK-IDDRC) P50 HD103556 (T.A. and Lane Strathearn, PI), the Roy J. Carver Directorship (T.A.), NARSAD Young Investigator Grant 32261 (J.K.), Interdisciplinary Graduate Program in Genetics at University of Iowa (Y.V.), NIH grant R01 MH 087463 (T.A.), NIH grant R01 DA 056113 (T.A.), Simons Foundation Autism Research Initiative (SFARI) grant 345034 (T.A.), NIH grant T32 GM067795 (B.K.), NIH grant F31 MH134542 (B.K.), NIH grant R01 MH115030 (M.F.), Eagles Autism Challenge (M.F. & T.N.-J.) and the Andrew H. Woods Professorship (T.N-J.).

The Neural Circuits and Behavior Core in the Iowa Neuroscience Institute provided equipment, facilities, and consultations services to support investigators in performing behavioral tasks. The Iowa Institute of Human Genetics provided snRNA sequencing services. A Carver College of Medicine / Holden Comprehensive Cancer Center Flow Cytometry Facility at the University of Iowa provided cell sorting service for snRNA sequencing. The facility is funded through user fees and the generous financial support of the Carver College of Medicine, Holden Comprehensive Cancer Center, and Iowa City Veteran's Administration Medical Center. Dr. Jocelyne Caboche, Sorbonne University, kindly provided AAV-ENK-CRE and AAV-PPTA-CRE virus. Dr. Joseph F. Lynch III, University of Iowa, helped maintain mouse lines. We thank Deaven Denis and Tasha Gilkison, (University of Iowa) for their technical assistance.

Author contributions

T.A. designed and supervised the study with input from J.K., A.A.M., M.V.F., K.T.B., and T.N-J. J.K. performed snRNA-seq experiments with assistance from S.C. Y.V. conducted the bioinformatics analysis with support from J.K. J.K. carried out the behavioral experiments and analyzed the data with assistance from B.K., S.L.F., and C.A. J.K. also performed the fiber photometry experiments and analyzed the data with assistance from B.K. and S.L.F. R.R. and M.F.D. performed electrophysiology experiments and analyses with assistance from J.K. T.A., A.A.M., M.V.F., K.T.B., and T.N-J. contributed to the discussion and interpretation of the results. J.K. wrote the manuscript with input from Y.V., B.K., R.R., and M.F.D. All authors read and approved the final manuscript.

Competing interests

Dr.T.A. served on the Scientific Advisory Board of EmbarkNeuro and was a scientific advisor to Aditum Bio and Radius Health. The remaining authors declare no competing interests.

Additional information

Supplementary information The online version contains supplementary material available at (https://doi.org/10.1038/s41467-025-68047-y).

Correspondence and requests for materials should be addressed to Ted Abel.

Peer review information *Nature Communications* thanks Adele Stewart, Donna Werling, and the other, anonymous, reviewer(s) for their contribution to the peer review of this work. A peer review file is available.